# cmgh

ORIGINAL RESEARCH

Loss of Mucosal p32/gC1qR/HABP1 Triggers Energy Deficiency and Impairs Goblet Cell Differentiation in Ulcerative Colitis

Annika Sünderhauf,[1] Maren Hicken,[1] Heidi Schlichting,[1] Kerstin Skibbe,[1] Mohab Ragab,[1] Annika Raschdorf,[1] Misa Hirose,[2] Holger Schäffler,[3] Arne Bokemeyer,[4] Dominik Bettenworth,[4] Anne G. Savitt,[5] Sven Perner,[6,7] Saleh Ibrahim,[2] Ellinor I. Peerschke,[8] Berhane Ghebrehiwet,[5] Stefanie Derer,[1,*] and Christian Sina[1,9,*]

[1]Division of Nutritional Medicine, University Hospital Schleswig-Holstein, Campus Lübeck, Lübeck, Germany; [2]Lübeck Institute of Experimental Dermatology and Center for Research on Inflammation of the Skin, University of Lübeck, Lübeck, Germany; [3]Division of Gastroenterology, Department of Medicine II, Rostock University Medical Center, Rostock, Germany; [4]Gastroenterology and Hepatology, Department of Medicine B, University Hospital Münster, Münster, Germany; [5]Department of Medicine, Stony Brook University, Stony Brook, New York; [6]Institute of Pathology, University Hospital Schleswig-Holstein, Lübeck, Germany; [7]Pathology, Research Center Borstel, Leibniz Lung Center, Borstel, Germany; [8]Department of Laboratory Medicine, Memorial Sloan Kettering Cancer Center, New York, New York; and [9]Division of Nutritional Medicine, 1st Department of Medicine, University Hospital Schleswig-Holstein, Campus Lübeck, Lübeck, Germany
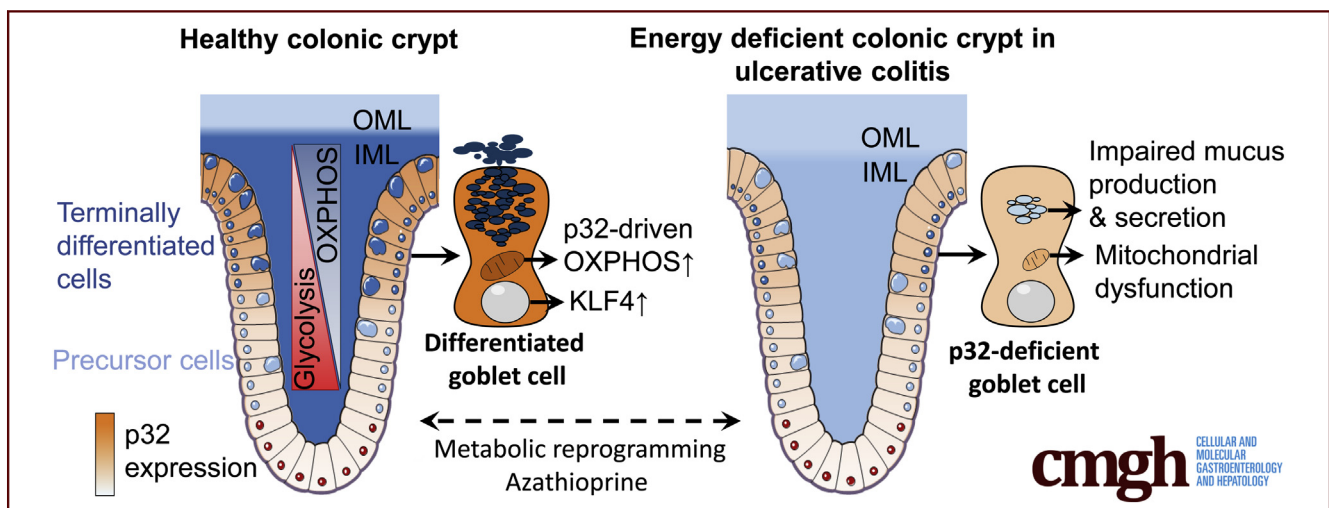
SUMMARY

Oxidative phosphorylation promoting p32 critically maintains mitochondria function essential for terminal goblet cell differentiation. Reduced colonic p32 expression in ulcerative colitis patients possibly explains a great range of disease-specific histopathological hallmarks.

BACKGROUND & AIMS: Cell differentiation in the colonic crypt is driven by a metabolic switch from glycolysis to mitochondrial oxidation. Mitochondrial and goblet cell dysfunction have been attributed to the pathology of ulcerative colitis (UC). We hypothesized that p32/gC1qR/HABP1, which critically maintains oxidative phosphorylation, is involved in goblet cell differentiation and hence in the pathogenesis of UC.

METHODS: *Ex vivo*, goblet cell differentiation in relation to p32 expression and mitochondrial function was studied in tissue biopsies from UC patients *versus* controls. Functional studies

were performed in goblet cell-like HT29-MTX cells *in vitro*. Mitochondrial respiratory chain complex V-deficient, ATP8 mutant mice were utilized as a confirmatory model. Nutritional intervention studies were performed in C57BL/6 mice.

RESULTS: In UC patients in remission, colonic goblet cell differentiation was significantly decreased compared to controls in a p32-dependent manner. Plasma/serum L-lactate and colonic pAMPK level were increased, pointing at high glycolytic activity and energy deficiency. Consistently, p32 silencing in mucus-secreting HT29-MTX cells abolished butyrate-induced differentiation and induced a shift towards glycolysis. In ATP8 mutant mice, colonic p32 expression correlated with loss of differentiated goblet cells, resulting in a thinner mucus layer. Conversely, feeding mice an isocaloric glucose-free, high-protein diet increased mucosal energy supply that promoted colonic p32 level, goblet cell differentiation and mucus production.

CONCLUSION: We here describe a new molecular mechanism linking mucosal energy deficiency in UC to impaired, p32-

dependent goblet cell differentiation that may be therapeutically prevented by nutritional intervention. *(Cell Mol Gastroenterol Hepatol 2021;12:229–250; https://doi.org/10.1016/j.jcmgh.2021.01.017)*

Ulcerative colitis (UC), as one main phenotype of inflammatory bowel disease (IBD), is a chronic, relapsing-remitting immune mediated disorder of the human gastrointestinal tract, in which inflammation is localized to the large intestine and restricted to the mucosa. While the exact pathophysiology is still not fully understood, genetic, environmental, and immune-mediated factors contribute to disease onset and recurrence in UC. Loss of intestinal epithelial and mucus barrier integrity leading to bacterial translocation is commonly accepted as a major cause of inflammation.[1] Correct cellular differentiation, which is pivotal for the cryptic architecture and thus barrier integrity, is a highly energy demanding process,[2] strongly suggesting that mitochondrial dysfunction plays a key role in both the onset and recurrence of the disease. Of main interest, mitochondrial dysfunction in epithelial cells, defective goblet cell differentiation, and mucus depletion in UC have been independently reported in several studies.[3–9] Nevertheless, mechanistic evidence linking cellular energy metabolism to goblet cell differentiation and UC pathogenesis is still missing.

Cells of the colonic mucosa utilize different mechanisms to maintain their energy homeostasis. Energy generation in cells of the lower third of the crypt (eg, intestinal stem cells) mainly depend on glycolysis, while short-chain fatty acids (SCFAs) inhibit stem and progenitor cell proliferation.[10,11] In contrast, differentiated postmitotic cells of the upper third of the crypt (eg, goblet cells) maintain their energy level through mitochondrial β-oxidation of SCFAs such as butyrate and the oxidative phosphorylation (OXPHOS) system.[2,11,12] We recently reported a cellular mechanism, whereby caspase-1–dependent cleavage of p32, a protein that critically maintains OXPHOS function, induces a metabolic shift from mitochondrial OXPHOS to cytosolic aerobic glycolysis.[13] This metabolic shift led to an enhancement of cell proliferation and a decrease in cell differentiation of cancer cells and is potentially involved in the transition of transient amplifying cells into postmitotic cells.

In the intestinal crypt, differentiation of goblet cells occurs along the metabolic trajectory of shifting energy source. Secretory precursor cells in the transit-amplifying zone are characterized by high expression of atonal basic helix-loop-helix transcription factor 1 (ATOH1) (also referred to as HATH1 in humans and Math1 in mice)[14] and further by high level of SAM pointed domain-containing Ets transcription factor 1 (SPDEF1).[15] Kruppel-like factor 4 (KLF4) expressing, terminally differentiated goblet cells are particularly specialized in the production and secretion of highly glycosylated proteins, so called mucins, with mucin 2 (MUC2) being the most abundant in the colon and small intestine. Notably, *klf4*-deficient mice display defective goblet cell differentiation with a decrease of about 90% of colonic goblet cells.[16] Reduced numbers of goblet cells in line with colonic mucus depletion have been suggested as histological hallmarks of UC.[6] Gersemann et al[8] showed that induction of goblet cell differentiation during inflammation is impaired in UC but not in Crohn's disease (CD). Furthermore, differentiation defects of intestinal stem cells have been found to be accompanied by a barrier dysfunction, leading to intestinal inflammation or cancer development.[17]

The OXPHOS system has been found to be highly active in cells of the upper part of the intestinal crypt.[2] Therefore, differentiated goblet cells are expected to be highly affected by reduced OXPHOS activity. Supporting this hypothesis, we recently published that loss of OXPHOS-stabilizing p32 by inflammasome-driven cleavage reduces goblet cell differentiation state in vitro.[13]

In 1980, Roediger[3] hypothesized that pathogenesis of UC is linked to energy deficiency. More specifically, Roediger found reduced butyrate oxidation rates in isolated colonocytes from UC patients compared with healthy control subjects. Furthermore, 2 independent studies reported reduced mitochondrial respiratory chain complex activity accompanied by mucosal ATP depletion in UC patients.[4,5] Interestingly, alterations in all 3 studies were already present in noninflamed tissue, implicating mitochondrial dysfunction as a pathophysiological cause, rather than a consequence, in UC.

The ubiquitous nuclear encoded multifunctional protein p32 critically maintains OXPHOS and was independently identified as a subunit of the human pre–messenger RNA (mRNA) splicing factor SF2,[18,19] as C1qbp (complement component 1q binding protein) (gC1qR [globular C1q receptor]),[20] and as HABP1 (hyaluronic acid binding protein).[21] p32 expression is integral to mitochondrial energy maintenance, with energy generation via OXPHOS being nearly absent in *p32* knockout cells[13,22] and *p32*-deficient mice being embryonic lethal.[23] Cumulative data indicate that one of the major functions of p32 is to maintain mitochondrial function by regulating mitochondrial protein translation.[23,24]

Taken together, we hypothesized p32 to be involved in the maintenance of the metabolic trajectory within the intestinal crypt, thereby enabling the metabolic switch from glycolysis to mitochondrial OXPHOS, which is necessary for terminal differentiation of intestinal stem cells toward goblet cells. Because mitochondrial dysfunction and defects in goblet cell differentiation have been attributed to UC pathogenesis, we aimed at investigating colonic expression of p32 in UC patients, as well as studying mechanistic backgrounds and possible modulation of OXPHOS-driven goblet cell differentiation.

Results

UC Patients in Remission Display Decreased Colonic p32 Expression, Increased Glycolysis, and Cellular Energy Deficiency

Stem cells in the lower part of the colonic crypt are mainly dependent on glycolysis, while there is a gradient toward an increase in energy generation via OXPHOS toward the differentiated cells at the tip of the crypt.[2,10,12] Cellular differentiation occurs alongside this gradient of shifting energy source (Figure 1A), and we postulated p32, as a main driver of mitochondrial OXPHOS, to be involved in its maintenance. Indeed, p32 is highly expressed in the upper part of the colonic crypt, together with mitochondrial marker TOMM22 and goblet cell differentiation marker KLF4 (Figure 1B and C). When p32 mRNA expression was analyzed in colonic biopsies obtained from UC patients in remission and non-IBD control subjects, we found significantly reduced p32 level in UC (Table 1, Figure 1D). At least 2 isoforms of p32 have been described, 1 encoding and 1 lacking the mitochondrial leader sequence in exon 1.[25] Hence, we investigated exon expression in a subset of intestinal biopsies from 10 non-IBD control subjects and 9 UC patients in remission. Expression of all exons, and therefore most likely all isoforms, of the p32 transcript was reduced in the intestine of UC patients compared with non-IBD control subjects (Figure 1E). Detection rates of the p32 exon 1 and exon 1–2 transcripts were more than 100-fold lower than for all other p32 exons when quantified by the dCt method. This was at least partially due to low binding capacity of corresponding anti-p32 probes as revealed by binding assays of these probes against a human full-length p32 plasmid (Figure 1F).

Owing to the fact that mitochondrial function is highly affected by aging[26] and various therapeutic regiments, we related p32 mRNA expression to patients' age and tested for potential influences of commonly prescribed therapeutics within our cohort such as prednisolone, mesalazine, and azathioprine. p32 mRNA expression did not correlate with age in either non-IBD control subjects or UC patients (Figure 1G). In line with previous studies, which showed azathioprine to impair cell proliferation,[27] azathioprine treatment was associated with higher p32 mRNA level in UC patients, an effect observed under neither mesalazine nor prednisolone therapy (Figure 1H and I). Therefore, biopsies from patients receiving azathioprine treatment were excluded from data presented in Figures 1D, E, and J and 2.

To investigate whether differences in p32 mRNA level are also reflected on protein level, a set of 10 colonic biopsies collected from non-IBD patients was compared with 9 colonic biopsies collected from UC patients in remission via immunohistochemistry staining of the p32 protein (clone EPR8871). p32 staining was densitometrically quantified in the upper third of the crypt and revealed a significantly lower p32 positive area in UC patients compared with non-IBD control subjects (Table 1, Figure 1J). Further, UC patients displayed increased L-lactate level in plasma and serum samples compared with non-IBD control subjects as well as high phosphorylation of AMPK (adenosine monophosphate kinase) in colonic biopsies, pointing to increased glycolysis activity and mucosal energy deficiency in UC patients (Table 2, Figure 2A–C).

Colonic Goblet Cell Differentiation Is Impaired in UC Patients in Remission and Goblet Cell Number Decreases With Increasing Degree of Inflammation

High glycolytic activity characterizes cell metabolism in proliferating precursor cells, rather than in nondividing differentiated cells.[10] Because goblet cell function has been previously proposed to be impaired in UC,[3,7,8] we focused on analyzing differentiation status of this cell entity. Interestingly, expression of terminal goblet cell differentiation marker KLF4 was significantly downregulated in colonic biopsies (hepatic flexure to sigmoid colon) from UC patients in remission compared with non-IBD control subjects (Figure 2D). Additionally, colonic KLF4 mRNA expression significantly correlated with p32 mRNA expression (Figure 2E), supporting the hypothesis that impaired terminal goblet cell differentiation in UC is a result of defective energy generation via p32-driven OXPHOS. Meanwhile, transcript levels of goblet cell precursor markers ATOH1 and SPDEF1 were not statistically altered (Figure 2D).

In the next set of experiments, we analyzed p32 expression and goblet cell appearance in noninflamed and inflamed tissue sections of UC patients in remission or active disease. Inflammasomes, as part of the innate immune system, are responsible for the initiation of inflammatory responses, mediated by the activation of caspase-1 among others.[28] We have recently published that active caspase-1 cleaves p32 at 2 distinct sites (exon 1–2 junction and in exon 5), thereby preventing mitochondrial import of p32. This mechanism results in a shift in energy generation of tumor cells from OXPHOS towards aerobic glycolysis (Figure 3A) and abrogation of differentiation of goblet cell–like HT29-MTX cells, in vitro.[13] p32 levels were not altered in UC tissue biopsies from inflamed vs noninflamed regions, when analyzing mRNA expression in paired biopsies or p32 protein expression utilizing an anti-p32 antibody detecting total p32 (binding to epitopes encoded by exon 5 before the C-terminal caspase-1 cleavage side (Table 1, Figure 3B and C)). In line with data published by Gersemann et al[8] in 2009, we did not observe induction of KLF4 expression in biopsies obtained from inflamed regions
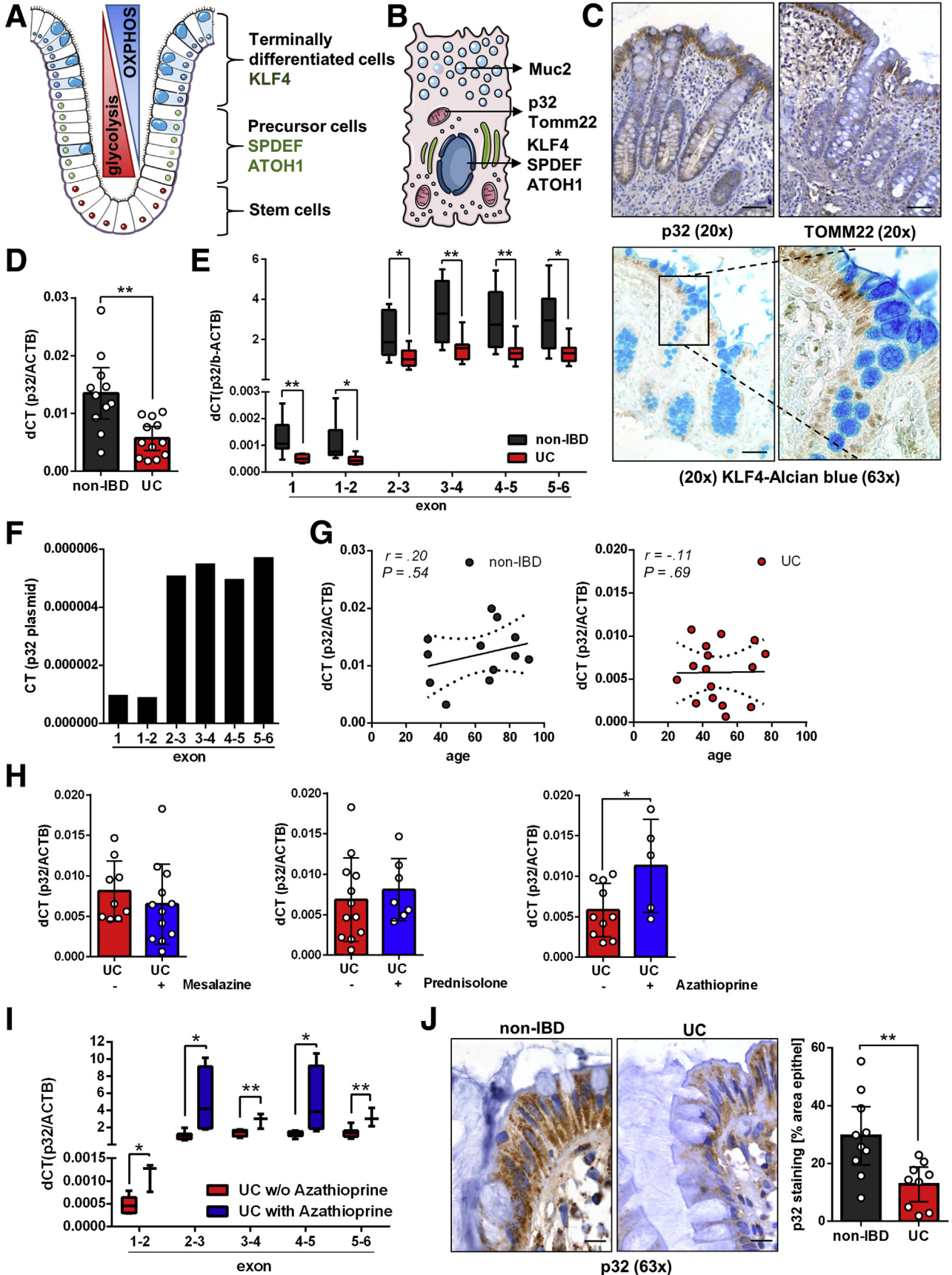
A — Terminally differentiated cells KLF4; Precursor cells SPDEF ATOH1; Stem cells; OXPHOS; glycolysis

B — Muc2; p32 Tomm22 KLF4 SPDEF ATOH1

C — p32 (20x)   TOMM22 (20x)   (20x) KLF4-Alcian blue (63x)

D — dCT (p32/ACTB); non-IBD; UC; **

E — dCT(p32/b-ACTB); non-IBD; UC; exon 1, 1-2, 2-3, 3-4, 4-5, 5-6

F — CT (p32 plasmid); exon 1, 1-2, 2-3, 3-4, 4-5, 5-6

G — dCT (p32/ACTB); $r = .20$ $P = .54$ non-IBD; age; $r = -.11$ $P = .69$ UC; age

H — dCT (p32/ACTB); UC − / UC + Mesalazine; UC − / UC + Prednisolone; UC − / UC + Azathioprine *

I — dCT(p32/ACTB); UC w/o Azathioprine; UC with Azathioprine; exon 1-2, 2-3, 3-4, 4-5, 5-6

J — non-IBD; UC; p32 staining [% area epithel]; non-IBD; UC; ** ; p32 (63x)

Table 1. Patient Characteristics of Native and Paraffin-Embedded Biopsies

	mRNA Expression			IHC Analysis		
Total number of patients included	39			24		
Non-IBD	11 (28.2)			10 (41.7)		
UC remission NI	18 (46.2)			9 (37.5)		
UC I	10 (25.6)			5 (20.8)		
Female/male/unknown						
Non-IBD	4 (36.4)/6 (54.5)/1 (9.1)			5 (50.0)/5 (50.0)/—		
UC remission NI	9 (50.0)/9 (50.0)/—			7 (77.8)/2 (22.2)/—		
UC I	5 (50)/5 (50)/-			3 (60.0)/2 (40.0)/—		
Age (unknown), y						
Non-IBD	62.2 ± 19.0 (1)			53.4 ± 11.3		
UC remission NI	52.4 ± 16.2 (1)			60.0 ± 13.5		
UC I	38.51 ± 13.4			51.6 ± 7.7		
Origin of biopsies	**Non-IBD**	**UC NI**	**UC I**	**Non-IBD**	**UC NI**	**UC I**
Cecum	—	4 (22.2)	—	—	—	—
Colon ascendens	2 (18.2)	2 (11.1)	—	—	—	—
Flexura hepatica	1 (9.1)	—	—	—	—	—
Colon transversum	1 (9.1)	1 (5.6)	—	1 (10.0)	—	—
Colon descendens	—	1 (5.6)	1 (10)	3 (30.0)	3 (33.3)	1 (20.0)
Colon sigmoideum	6 (54.5)	9 (50.0)	9 (90)	6 (60.0)	6 (66.7)	4 (80.0)
Rectum	1 (9.1)	1 (5.6)	—	—	—	—
Colon unclassified	—	—	—	1 (10.0)	1 (11.1)	—
Medication	**Non-IBD**	**UC NI**	**UC I**	**Non-IBD**	**UC NI**	**UC I**
Mesalazine/mesalazine klysmen	—	12 (66.7)	5 (50)	—	5 (55.6)	2 (40.0)
Prednisone	—	6 (33.3)	7 (70)	1 (10.0)	—	2 (40.0)
Azathioprine	—	5 (27.7)	1 (10)	—	—	—
Sulfasalazine	—	2 (11.1)	1 (10)	—	1 (11.1)	—
Tacrolimus	—	2 (11.1)	—	—	-	1 (20.0)
Budesonide klysmen	—	—	—	—	—	2 (40.0)
Metronidazole	—	—	3 (30)	1 (10)	—	1 (20.0)
Sirolimus	—	1 (5.6)	—	—	—	—
Hydrocortisone rectal foam	—	1 (5.6)	—	—	—	—
Olsalazine	—	1 (5.6)	—	—	—	—
Ciprofloxacin	—	—	—	3 (30.0)	1 (11.1)	1 (20.0)

NOTE. Values are mean ± SD or n (%), unless otherwise indicated.
I, inflamed; IBD, inflammatory bowel disease; IHC, immunohistochemistry; mRNA, messenger RNA; NI, noninflamed; UC, ulcerative colitis.

Figure 1. (*See previous page*). **UC patients in remission not receiving azathioprine display reduced colonic p32 level.** (*A*) A model for energy generation and goblet cell differentiation in the colonic crypt and (*B*) schematic subcellular localization of proteins of interest were generated by modifying images from Servier Medical Art.[53] (*C*) Representative immunohistochemistry staining of p32 (clone EPR8871), Tomm22, and KLF4 in paraffin-embedded human colonic biopsies. Scale bar = 50 μM. (*D*) p32 mRNA expression was measured by quantitative reverse-transcription polymerase chain reaction (qRT-PCR) in colonic biopsies from non-IBD and UC patients in remission. (*E*) p32 exon expression was analyzed by TaqMan assay. Non-IBD: n = 10; UC: n = 7 and 6 for exon 1 and exon 1–2, respectively, and n = 8–9 for all other exon junctions. (*F*) Binding of TaqMan probes to the p32 plasmid was analyzed by qRT-PCR. (*G*) Intestinal p32 transcript expression was correlated against age. (*H*) p32 mRNA level in colonic biopsies from UC patients in remission treated with or without mesalazine, prednisolone, or azathioprine was measured by qRT-PCR. (*I*) Exemplary measurement of patients receiving azathioprine or control treatment applying TaqMan probes for every exon-exon junction. UC w/o azathioprine n = 5 for exon 1–2 and n = 7–8 for all other exons; UC with azathioprine n = 3–4. (*J*) Representative immunohistochemistry staining and corresponding quantification[51] of p32 (clone EPR8871) expression in the upper part of the colonic crypt in paraffin-embedded biopsies from non-IBD control subjects and UC patients in remission. Scale bar = 10 μM. (*D, E*) Unpaired *t* test with Welch's correction; (*G*) Spearman's rank correlation coefficient; (*H–J*) unpaired *t* test; results are shown as (*D, J*) mean ± 95% CI, (*E, I*) box-and-whisker plot min to max, or (*H*) mean ± SD. *$P \le .05$, **$P \le .01$.

Table 2. Patient Characteristics Serum Samples and Western Blot Biopsies

	Serum/Plasma	Western Blot Analysis	
Total number of patients included	**33**	**9**	
Non-IBD	17 (51.5)	5 (55.6)	
UC remission	16 (48.5)	4 (44.4)	
Female/male			
Non-IBD	9 (52.9)/8 (47.1)	3 (60.0)/2 (40)	
UC remission	7 (43.8)/9 (56.3)	1 (25)/3 (75)	
Age (unknown), y			
Non-IBD	30.3 ± 9.7	49.8 ± 24.2	
UC remission	43.8 ± 7.7 (10)	60.15 ± 17.04	
Origin of biopsy	Not applicable	**Non-IBD**	**UC**
Cecum		—	1 (25.0)
Colon ascendens		1 (20.0)	1 (25.0)
Flexura hepatica		1 (20.0)	—
Colon descendens		1 (20.0)	1 (25.0)
Colon sigmoideum		1 (20.0)	—
Rectum		1 (20.0)	1 (25.0)
Medication	**UC**	**UC**	
Mesalazine/mesalazine klysmen	15 (93.8)	2 (50)	
TNF-α inhibitors	8 (50.0)	—	
Prednisone	1 (6.3)	2 (50)	
Vedolizumab	3 (18.8)	—	
Budesonide klysmen	2 (12.5)	—	
Thiopurines	2 (12.5)	—	
Hydrocortisone rectal foam	—	1 (25)	
Ciprofloxacin	—	1 (25)	
Sulfasalazine	—	1 (25)	
Tacrolimus	—	1 (25)	

NOTE. Values are n (%) or mean ± SD, unless otherwise indicated.
IBD, inflammatory bowel disease; TNF-α, tumor necrosis factor α; UC, ulcerative colitis.

of patients with active UC compared with noninflamed biopsies from UC patients in remission (Table 1, Figure 3D). Of note, protein expression of pro-caspase-1 was reduced in inflamed but not in noninflamed tissue areas of UC patients indicating inflammasome activation in respective regions. Consistent with reported caspase-1–induced p32 cleavage, binding of an antibody against p32 exon 6 was reduced in UC inflamed tissue sections compared with non-IBD control subjects in a disease activity–dependent manner. Furthermore, blinded evaluation of PAS-Alcian blue staining revealed reduced staining intensity of goblet cell granules in UC noninflamed tissue compared with non-IBD control subjects under basal conditions. The amount of mucus-filled goblet cells was reduced under low-grade inflammation and further decreased with increasing degree of mucosal inflammation (Table 1, Figures 3E and 4). Overall, these findings support our previous observation that caspase-1 cleavage of p32 leads to abrogation of goblet cell differentiation,[13] thereby further reducing mitochondria-localized and functional p32 and differentiated goblet cells in UC.

Goblet Cell Differentiation Is Dependent on OXPHOS and p32 In Vitro

To test our hypothesis that OXPHOS-driven goblet cell differentiation in the intestinal crypt is dependent on p32, we next screened a range of human colorectal carcinoma cell lines for expression of goblet cell differentiation markers, MUC2, Mucin5AC (MUC5AC), and p32. HT29-MTX cells depicted high basal mRNA level of SPDEF1, indicating a goblet cell precursor phenotype as well as MUC5AC but not MUC2. While DiFi cells displayed high levels of both ATOH1 and KLF4, the analyses of T84 cells indicated terminal differentiation reflected by high expression of KLF4 and MUC2. All these 3 goblet cell–like cell lines similarly expressed p32 mRNA (Figure 5A). To find an inducible cell line model to study dependency of goblet cell differentiation on mitochondrial activity in vitro, β-oxidation and hence OXPHOS in HT29-MTX, T84, and DiFi cells was boosted through stimulation with the SCFA butyrate in the presence or absence of the proinflammatory stimulus lipopolysaccharide, frequently present in the intestine (Figure 5B and C).
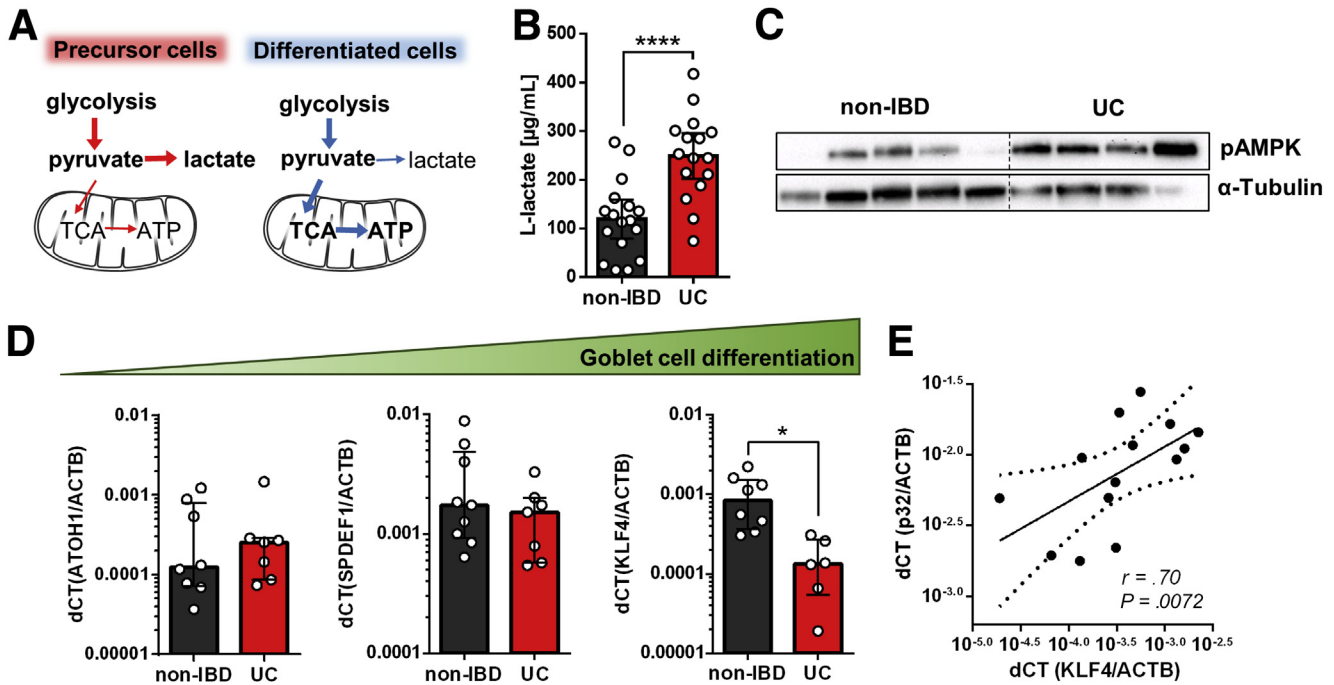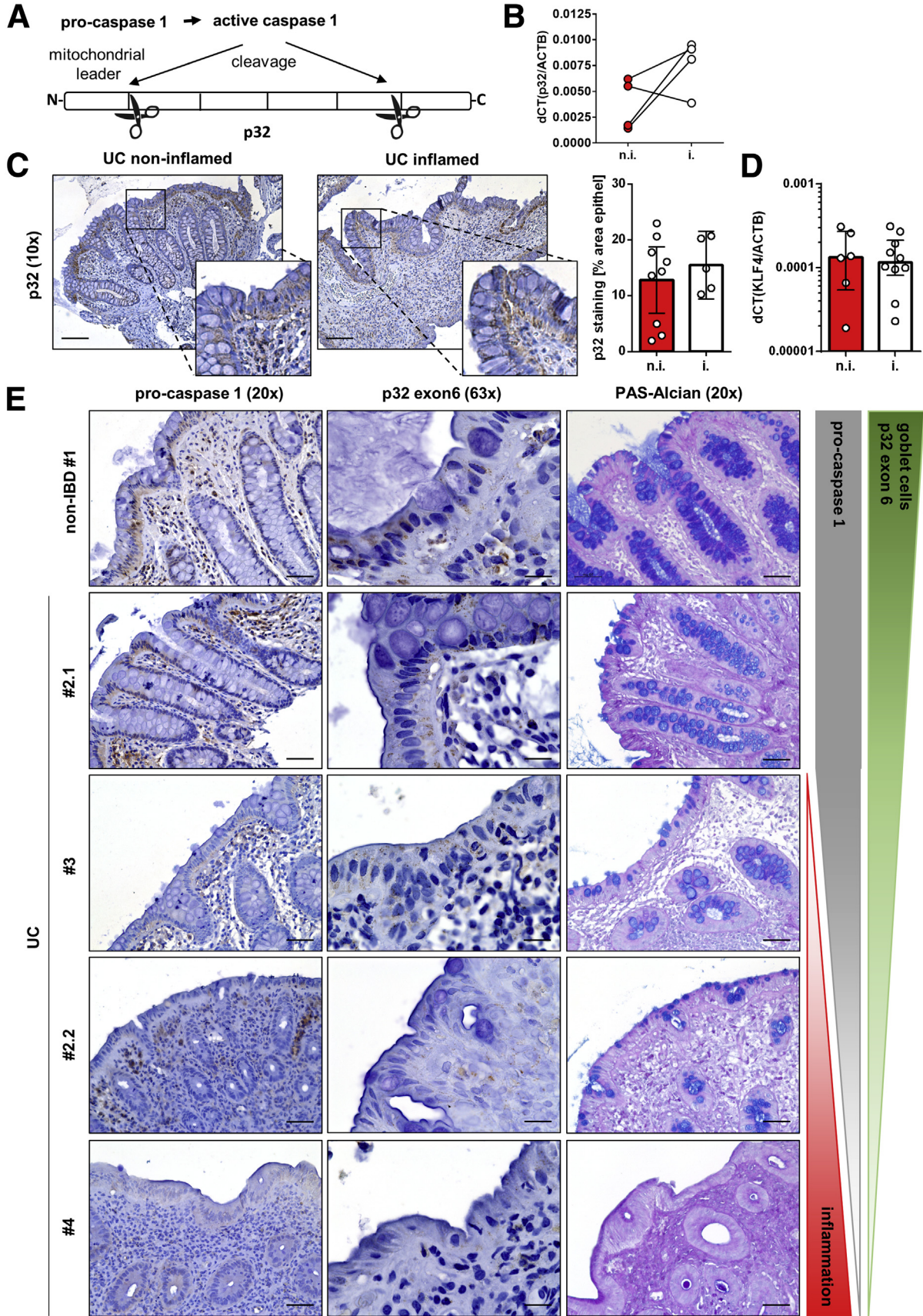
Figure 2. UC patients in remission display mucosal energy deficiency and impaired goblet cell differentiation.
(*A*) Comparison of energy generation cells of the transit amplifying and differentiated cell zone. (*B*) L-lactate level were measured in serum or plasma samples and (*C*) Western blot experiments were performed in colonic biopsies from non-IBD control subjects and UC patients in remission. (*D*) Expression of transcripts of interest was performed by qRT-PCR in colonic biopsies from non-IBD control subjects and UC patients in remission. (*E*) Colonic p32 mRNA expression was correlated against KLF4 mRNA expression in non-IBD control subjects and UC patients in remission. (*B*) Unpaired *t* test; (*D*) unpaired *t* test with Welch's correction; (*E*) Spearman's rank correlation coefficient; results are shown as (*B*) mean ± 95% CI or (*D*) median ± interquartile range. *$P \leq .05$, ****$P \leq .0001$.

Butyrate stimulation induced terminal goblet cell differentiation of HT29-MTX but not of T84 or DiFi cells, reflected by induction of KLF4 expression, which was abrogated in the presence of lipopolysaccharide (Figure 5*C*). Butyrate-triggered terminal goblet cell differentiation of HT29-MTX cells was accompanied by an increase in oxygen consumption rate (OCR) but not in extracellular acidification rate (ECAR) (Figure 5*D*),[13] underlining the importance of a metabolic switch toward OXPHOS in goblet cell differentiation. Furthermore, differentiated HT29-MTX cells displayed increased mucin granule formation, decreased cell proliferation, and enhancement of secreted Muc5AC (Figure 5*E*–*H*). Of note, p32 mRNA expression was not altered upon butyrate stimulation (Figure 5*I*). To test whether goblet cell differentiation is indeed dependent on p32, we performed silencing RNA (siRNA)–induced silencing experiments in HT29-MTX cells. Of main interest, induction of goblet cell differentiation via butyrate was abrogated in p32-silenced HT29-MTX cells accompanied by increased lactate level, indicating a switch in energy metabolism toward aerobic glycolysis. Thus, supporting the idea that p32 maintains mitochondrial function and thereby ensures goblet cell differentiation (Figure 5*J* and *K*). OXPHOS is a lot more efficient in the production of ATP compared with aerobic glycolysis. Therefore, we proposed a pivotal role for cellular energy supplied by the mitochondrial OXPHOS system not only for goblet cell differentiation, but also for

mucus secretion. To test this hypothesis, HT29-MTX cells were first terminally differentiated by postconfluent growth,[29] followed by stimulation with OXPHOS complex V blocker oligomycin or the uncoupling agent DNP (2,4-dinitrophenol) (Figure 6*A* and *B*). As expected, blocking of OXPHOS function by oligomycin resulted in a shift of cellular energy metabolism from OXPHOS to glycolysis (Figure 6*C*). Moreover, mucus secretion was impaired by oligomycin as well as by DNP, reflected by a dose-dependent downregulation of secreted but not intracellular Muc5AC (Figure 6*D*–*G*), supporting the idea that mucus secretion is a highly energy demanding process enabled by efficient OXPHOS activity.

ATP8 mutant Mice Display Low Colonic p32 Expression in Concert With Loss of OXPHOS and Goblet Cells

To investigate the observed UC phenotype of low colonic p32 level, energy deficiency, and defective goblet cell differentiation in a mouse model, we applied conplastic respiratory chain complex V mutant mice. These mice carry a mutation in the mitochondrial encoded ATP8-synthase resulting in diminished respiratory capacity and ATP production with parallel induction of energy generation via nonmitochondrial glycolysis in various cell entities.[30–32] (Figure 7*A*). ATP8 mutant mice did not
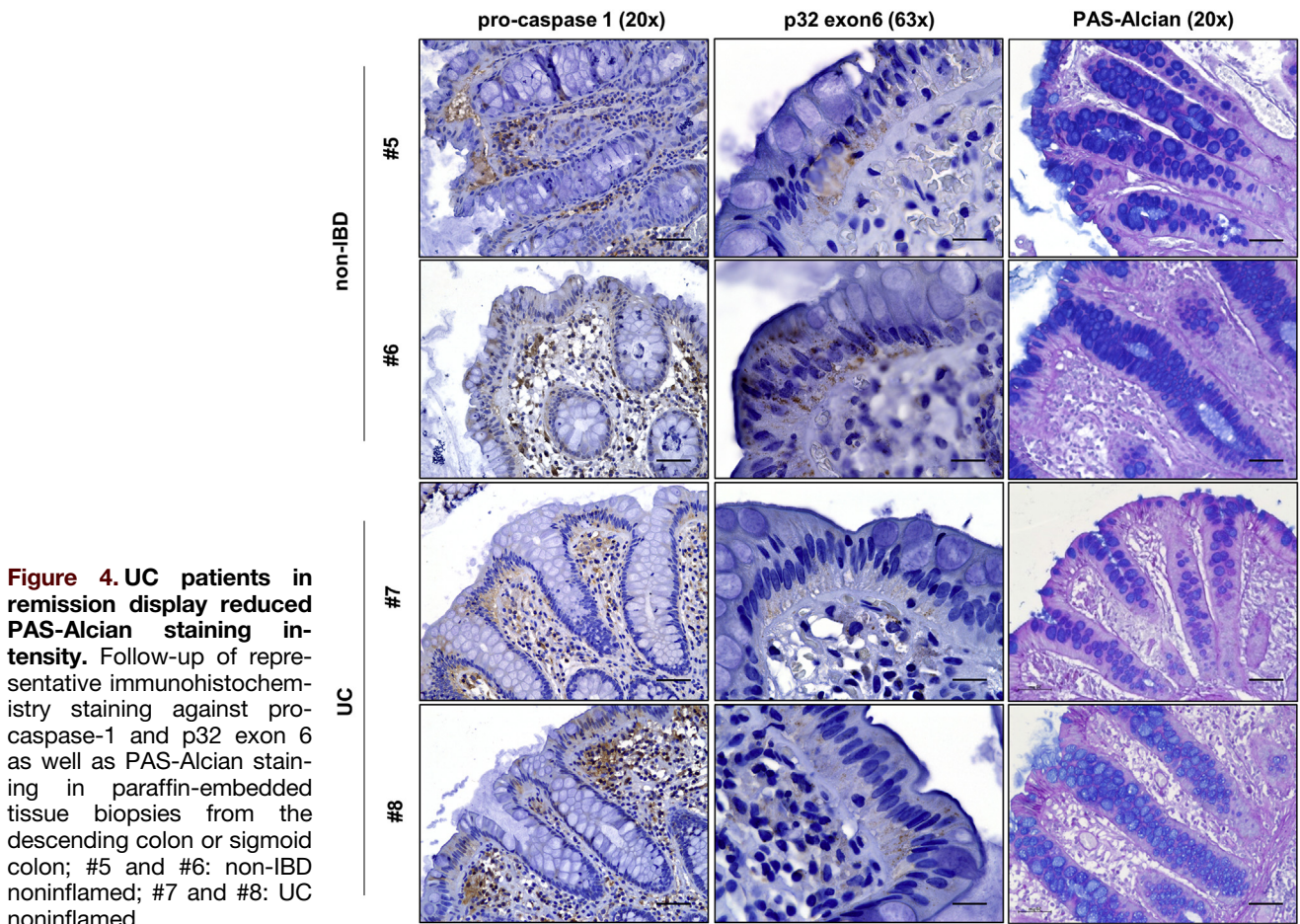
**Figure 4. UC patients in remission display reduced PAS-Alcian staining intensity.** Follow-up of representative immunohistochemistry staining against pro-caspase-1 and p32 exon 6 as well as PAS-Alcian staining in paraffin-embedded tissue biopsies from the descending colon or sigmoid colon; #5 and #6: non-IBD noninflamed; #7 and #8: UC noninflamed.

exhibit signs of colonic inflammation under basal conditions, as defined by an inconspicuous colonoscopy and similar mRNA expression of cxcl1/keratinocyte chemo-attractant in colonic biopsies compared with wild-type (WT) B6 mice (Figure 7B and C). Furthermore, intestinal barrier integrity was still intact, with comparable level of immunoglobulin A (IgA) in fecal samples of FVB mutant compared with B6 WT mice and similar amounts of mucosa attached bacteria in colonic biopsies (Figure 7D and E). Specifically, we found that ATP8 mutant mice displayed reduced p32 mRNA expression and diminished p32 protein level especially in differentiated intestinal epithelial

cells in the upper part of colonic crypts (Figure 7F and G), while serum L-lactate levels were similar between strains (Figure 7H). In line with the phenotype observed in UC patients, loss of p32 in ATP8 mutant mice was associated with altered colonic goblet cell differentiation represented by decreased klf4 mRNA expression, diminished mucus filling of goblet cells and a reduced thickness of the colonic mucus layer. As observed in the human colon, klf4 mRNA expression significantly correlated with p32 mRNA expression in colonic samples from B6 WT and ATP8 mutant mice (Figure 7I–K). Expression of atoh1 and spdef1 was not altered, which was comparable to

Figure 3. (*See previous page*). Goblet cell loss correlates with inflammasome activation and decrease of full-length p32 level in active UC. (A) Schematic visualization of p32 cleavage by active Caspase-1. (B) p32 mRNA expression in paired biopsies from noninflamed and inflamed intestinal tissue sections were quantified by qRT-PCR. (C) Representative immunohistochemistry staining and corresponding quantification[51] of p32 protein expression (clone EPR8871, anti-p32 exon 5) in the upper part of the colonic crypt in paraffin-embedded biopsies from noninflamed and inflamed colonic tissue sections from UC patients. Scale bar = 100 μM. (D) KLF4 mRNA expression was quantified by qRT-PCR in noninflamed colonic biopsies from UC patients in remission and inflamed colonic biopsies from UC patients with active disease. (E) Representative immunohistochemistry staining against pro-caspase-1 and p32 exon 6 as well as PAS-Alcian staining in paraffin-embedded tissue biopsies from the descending colon or sigma; #1: non-IBD noninflamed; #2.1: UC noninflamed; #3: UC low-grade inflammation; #2.2: UC medium-grade inflammation; #4: UC high-grade inflammation. Representative images from 8 biopsies each categorized as non-IBD control subjects or UC noninflamed and 5 UC inflamed samples are displayed. Scale bar = 50 μM. Results are shown as (C) mean ± 95% CI or (D) median ± interquartile range. i., inflamed; n.i., noninflamed.
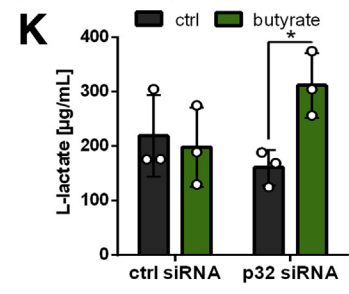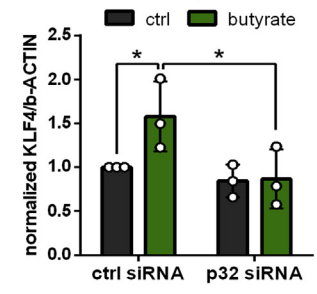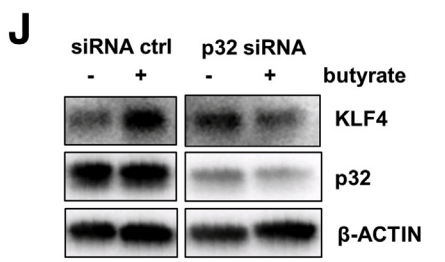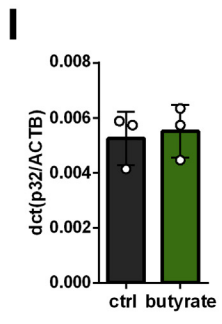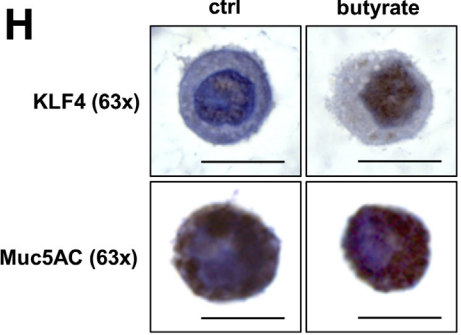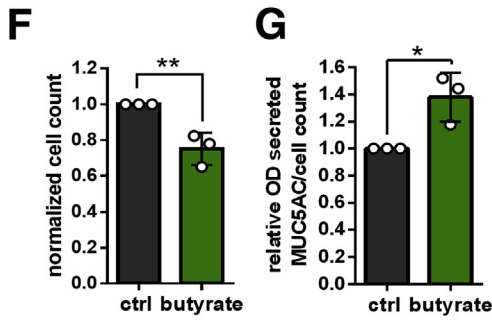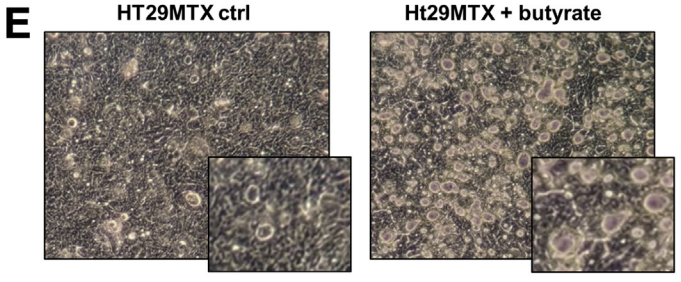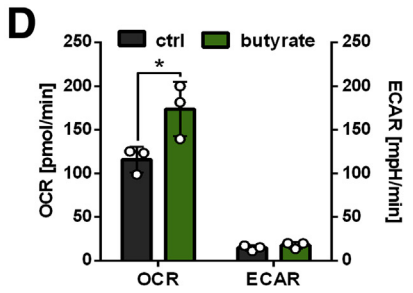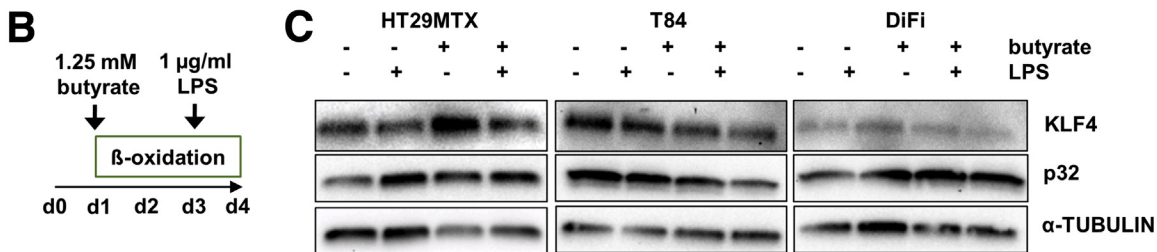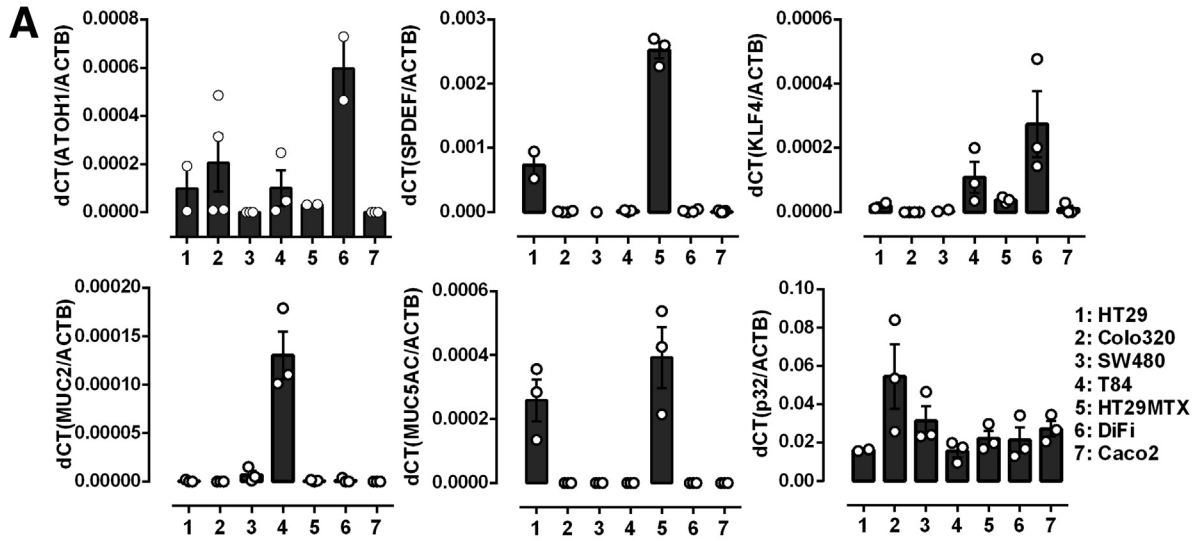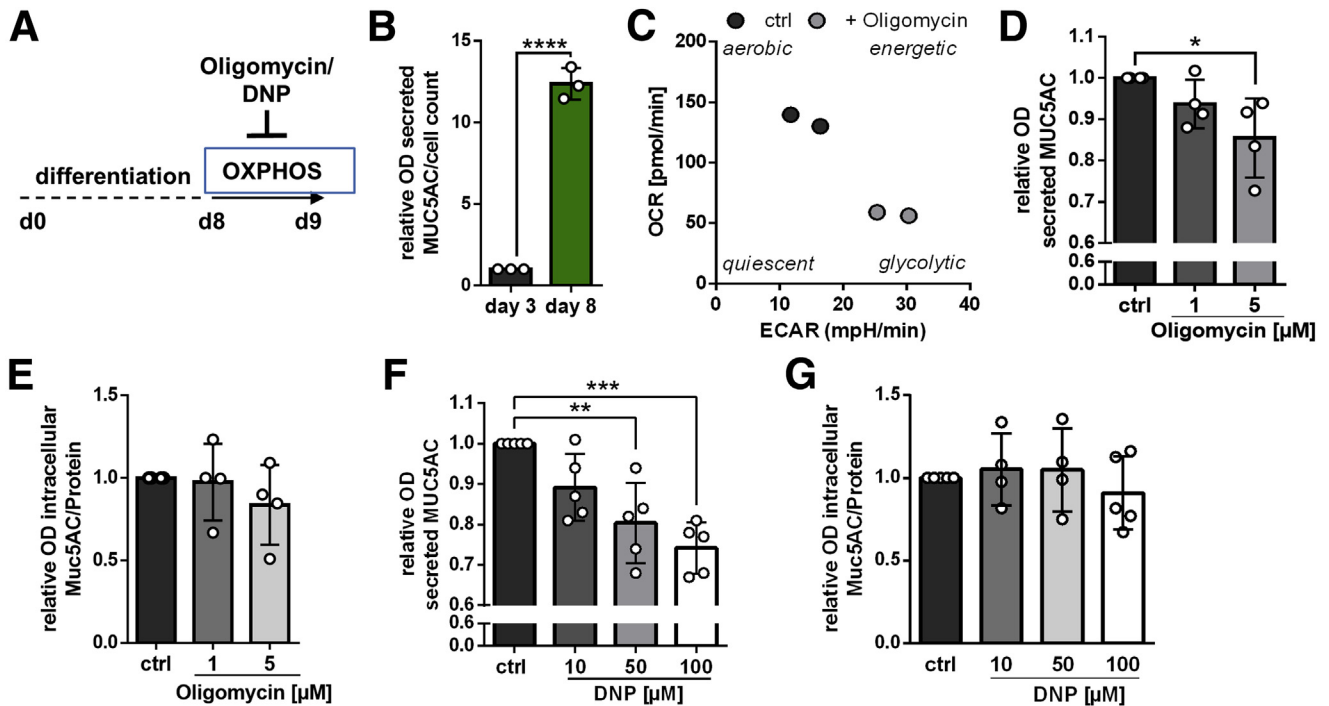
Figure 6. Mucin secretion is dependent on energy supplied by mitochondrial respiration. (*A*) Graphical setup of cell culture experiments. (*B*) HT29-MTX cells were grown for 3 or 8 days. Muc5AC was measured by direct ELISA in cell culture supernatants, was normalized to cell count, and is shown as fold change to 3 days grown HT29MTX. (*C*) Seahorse measurement of HT29-MTX cells before and after 2 μM oligomycin injection. Muc5AC level in the cell culture supernatant after 24-hour stimulation with (*D*) oligomycin or (*F*) DNP were measured by ELISA and normalized to each control. Intracellular Muc5AC level of (*E*) oligomycin or (*G*) DNP-stimulated HT29-MTX cells were measured by direct ELISA in native protein isolates. Intracellular Muc5AC level was normalized to corresponding protein concentrations. (*B*) Unpaired *t* test; (*D, F*) 1-way analysis of variance with Tukey's post hoc test for multiple comparisons; results are shown as mean ± SD. *$P \leq$ .05, **$P \leq$ .01, ***$P \leq$ .001, ****$P \leq$ .0001.

observations in UC patients (Figure 7*I*). Furthermore, expression of the proliferation marker ki67 and the stem cell marker lgr5 were not different in colonic biopsies from ATP8 mutant mice (Figure 7*L*). Taken together, we here present a mouse model with low intestinal p32 level and diminished energy generation via OXPHOS to depict reduced numbers of terminally differentiated goblet cells in the colon, strengthening the notion that especially goblet cell differentiation is highly sensitive to mitochondrial dysfunction.

A Glucose-Free Nutritional Intervention Promotes Colonic p32 Expression and Goblet Cell Differentiation in Mice

Finally, we aimed to study regulation of goblet cell differentiation via the enhancement of intestinal p32 expression in a glucose-free, high-protein nutritional intervention in mice. Because availability of nutrients critically affects cellular metabolism,[33] we hypothesized that withdrawal of glucose from the diet and isocaloric replacement of glucose by the protein casein may result in a metabolic shift toward

Figure 5. (*See previous page*). **Goblet cell differentiation is dependent on p32 expression.** (*A*) Transcripts of goblet cell differentiation factors, mucins, and p32 were measured in colorectal cancer cell lines by qRT-PCR. (*B*) Graphical setup of cell culture experiments. (*C*) Western blot experiments were performed from whole protein extracts with respective antibodies in cells stimulated with 1.25-mM butyrate and/or 1-μg/mL lipopolysaccharide (LPS) (p32 clone EPR8871). (*D*) Basal OCR and ECAR were measured by Seahorse assay.[13] (*E*) Representative image of HT29-MTX cell growth characteristics. (*F*) Cell counts are presented as fold change for each individual experiment. (*G*) Muc5AC levels in the supernatant were measured by ELISA, were normalized to cell count, and are displayed as fold change for each individual experiment. (*H*) KLF4 and MUC5AC immunohistochemistry staining was performed in paraffin-embedded butyrate-stimulated or control HT29-MTX cells. Scale bar = 10 μM. (*I*) p32 mRNA expression in butyrate-treated or untreated HT29-MTX cells was measured by qRT-PCR. (*J, K*) For siRNA knockdown, HT29-MTX cells were stimulated with 50-nM p32 siRNA or respective control for 96 hours and butyrate for 72 hours. (*J*) Representative Western blot and quantification from whole protein extracts (p32 clone 60.11) and (*K*) L-lactate level from corresponding cell culture supernatants. (*D*) Paired *t* test; (*F, G*) unpaired *t* test; (*J, K*) uncorrected Fisher's test; data are shown as mean ± SD with the exception of (*A*) mean ± SEM. *$P \leq$ .05, **$P \leq$ .01.
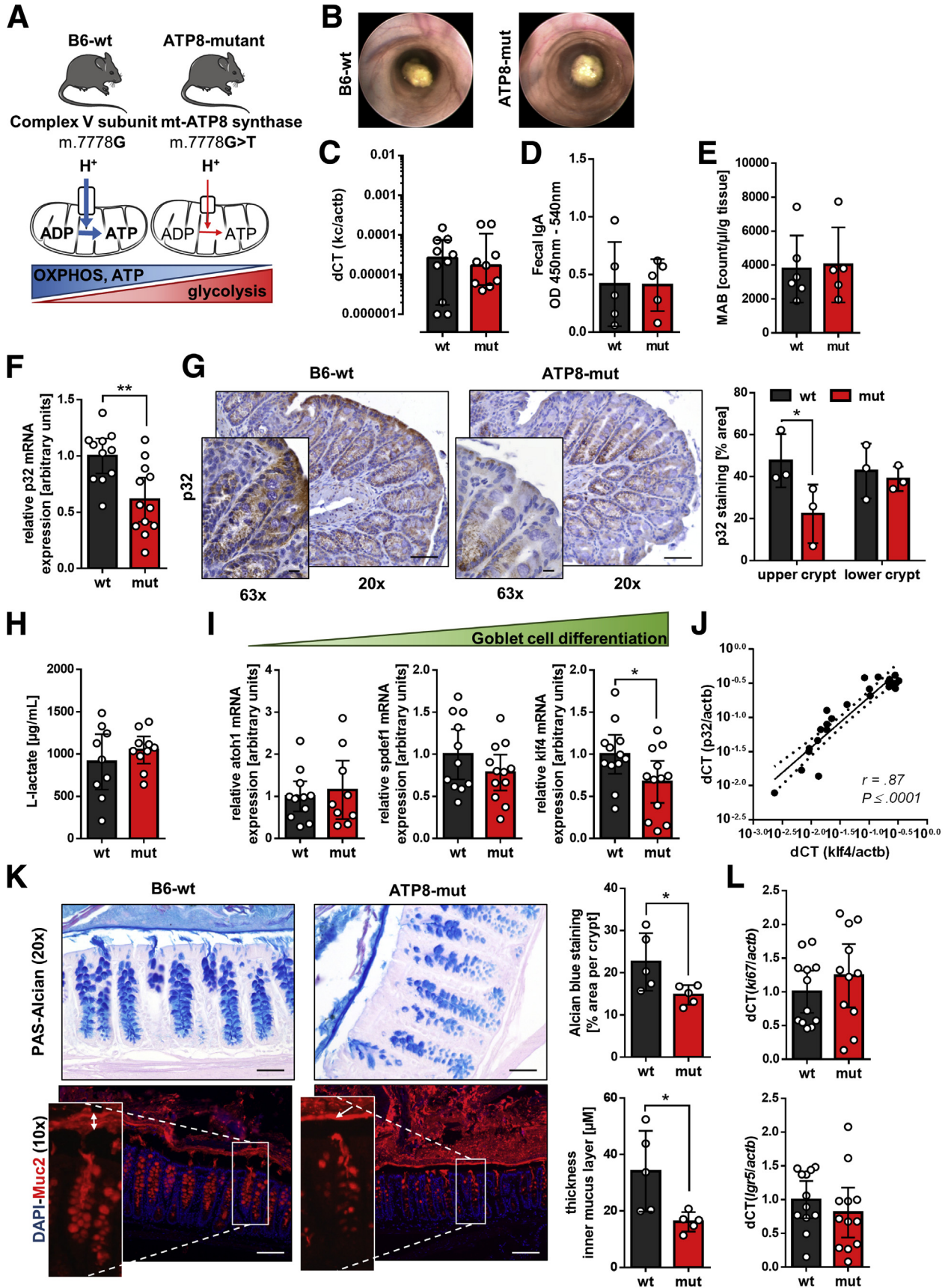
mitochondrial oxidation (Figure 8A). Adult C57BL/6 mice were fed a glucose-free high-protein (GFHP) diet or an isocaloric control diet for an average of 70 days before organ sampling and molecular analysis. Food consumption, body weight, serum glucose level, and lactate level were similar between diets (Figure 8B–E). Of main interest, GFHP diet–fed mice exhibited increased p32 protein level in the upper part of the colonic crypt, which was not due to elevated p32 mRNA level (Figure 8F–H). Simultaneously, GFHP diet–fed mice displayed high colonic energy level, reflected by low phosphorylation of AMPK (Figure 8H). Eventually, we tested whether enhanced p32 expression would also result in enhanced goblet cell differentiation. In comparison with control mice, increased KLF4 mRNA and protein expression as well as a thicker colonic mucus layer were potent indicators for induction of terminal differentiation of goblet cells under GFHP diet (Figure 8I and J). Further, spdef1 as a marker for secretory progenitor cells tended to be reduced in GFHP diet mice (without statistical significance, $P \leq .06$), supporting the idea that p32 expression is pivotal for the transition from secretory precursors toward terminal differentiated goblet cells (Figure 8I). Expression of intestinal stem cell marker lgr5 and proliferation marker ki56 were unaltered upon GFHP diet (Figure 8K). Taken together, nutritional intervention by glucose restriction in the presence of high protein intake appears as a promising tool to enhance colonic p32, thereby improving cellular energy supply and finally promoting goblet cell differentiation.

Discussion

Within the colonic crypt, mitochondria maintain the energy gradient, which is necessary for efficient cell differentiation and proliferation and thereby critical in determination of epithelial cell fate.[2,10,12] Mitochondrial disturbance and dysfunction of goblet cells are hallmarks of UC pathology,[3–6,34] which presents as a multifactorial disease, in which inflammation is caused by a disruption of the colonic epithelial and mucus barrier. Terminally differentiated goblet cells have a pivotal role in the maintenance of intestinal barrier integrity, and their differentiation is presumably regulated by a metabolic switch from glycolysis to mitochondrial OXPHOS.[2,16] In order to understand the molecular basis and disease origin of UC, it is necessary to find the underlying cause of mitochondrial dysfunction and to unravel a potential link to impaired goblet cell function.

Both IBD subtypes, UC and CD, are disorders of the gastrointestinal tract, which display dysfunctional mitochondria. Nevertheless, while mitochondrial disturbance results in aberrant development of Paneth cells in CD,[35] we here present abrogation of goblet cell differentiation through insufficient mitochondrial respiration as a potential cause for disease development in UC. Impaired induction of goblet cell differentiation in inflamed UC but not CD has been previously reported.[8] Our data indicate that defective terminal differentiation of goblet cells is already present in noninflamed colonic tissue of UC patients in remission, defined by diminished mucus filling of goblet cells and reduced expression of terminal goblet cell differentiation marker KLF4 compared with non-IBD control subjects. In line with this tenet, reduced numbers of goblet cells and a defective colonic mucus layer enabling bacterial invasion were already published for UC patients in remission.[6,7,9,36] Very recently differentiation of intestinal stem cells into the secretory lineage has been proposed to depend on mitochondria by a mechanism involving FoxO (Forkhead box O) transcription factors and Notch signaling–regulated mitochondrial fission.[37] Data presented here suggest that loss of p32, which is postulated to be the main driver of OXPHOS, is the underlying cause of metabolic dysfunction and secondarily of defective goblet cell function in UC.

In addition to the observation that low p32 expression is accompanied by mitochondrial dysfunction and defective goblet cell maturation in UC, we present experimental evidence that induction of goblet cell differentiation is dependent on p32-regulated mitochondrial function in vitro. Stimulation of a mucus producing goblet cell–like cell line with the SCFA butyrate resulted in induction of OXPHOS and terminal differentiation. Of main interest, differentiation was abolished by p32 silencing, and mucus secretion was impaired after treatment with OXPHOS inhibitors. In line with these observations, polymorphisms in nuclear-encoded mitochondrial genes involved in ATP generation, namely uncoupling protein 2 (UCP2) and SLC22A5, encoding the OCNT2 (organic carnitine transporter 2), have been described as risk factors for UC.[38,39] In addition, inhibition of intestinal fatty acid β-oxidation as well as genetic ablation

---

Figure 7. (*See previous page*). **Mitochondrial dysfunction in mice is accompanied by defective goblet cell differentiation.** (*A*) Schematic overview of the mutation in subunit 8 of the ATP synthase in ATP8 mutant mice and published metabolic imbalance.[31,32] (*B*) Representative colonoscopy image (n = 3 mice per group). (*C*) Kc mRNA expression was measured by qRT-PCR. (*D*) Fecal IgA was determined by ELISA. (*E*) Mucosa-attached bacteria (MAB) were extracted from colonic tissue by hypotonic cell lysis, stained with a commercial bacterial stain, quantified by fluorescence-activated cell sorting analysis, and normalized to tissue weight. (*F, I, L*) Expression of transcripts of interest was performed by qRT-PCR in colonic biopsies from B6 WT and ATP8 mutant mice. Data were normalized to β-actin and are displayed as relative values to B6 WT mice for each sampling round. (*G*) Representative immunohistochemistry staining and according quantification[51] of p32 (clone EPR8871) expression in paraffin-embedded colonic biopsies of B6 WT and ATP8 mutant mice (n = 3 mice per group). Scale bar = 50 μM (20×), 10 μM (63×). (*H*) L-lactate levels were measured in serum samples from B6 WT and ATP8 mutant mice. (*J*) Colonic p32 mRNA expression was correlated against klf4 mRNA expression in B6 WT and ATP8 mutant mice. (*K*) Representative PAS-Alcian and Muc2 fluorescent staining with according quantification[51] in Carnoy's fixed colonic tissue samples from B6 WT and ATP8 mutant mice. Scale bar = 50 μM (PAS-Alcian), 100 μM (Muc2 IF). Arrow indicates inner mucus layer. (*F, G, I*) Unpaired *t* test; (*J*) Spearman's rank correlation coefficient; (*K*) unpaired *t* test with Welch's correction; results are shown as (*C*) median with interquartile range, (*D, E, G, K*) mean ± SD, or (*F, I, L*) mean ± 95% CI. *$P \leq .05$, **$P \leq .01$.
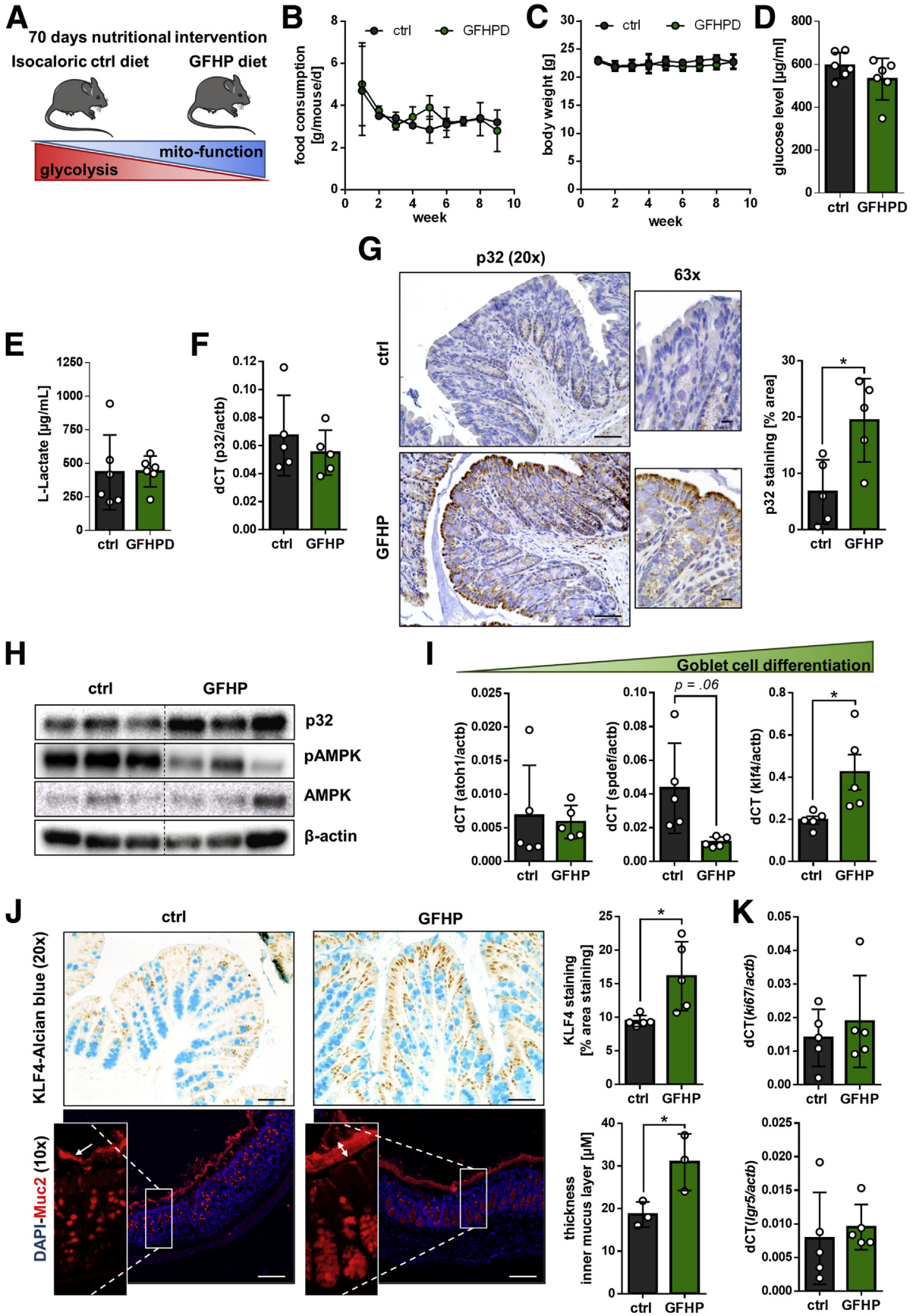
Table 3. Chow Composition as Provided by the Manufacturer

Diet composition	Isoenergetic control diet	Glucose-free high-protein diet
Casein, %	20	60
Brewer's yeast, %	—	2
Corn starch, %	28	—
Maltodextrin, %	14.5	—
Sucrose, %	10	—
Cellulose powder, %	15	19.5
L-cystine, %	0.3	0.3
Vitamin premixture, %	1	1
Minerals and trace elements, %	6	6
Choline chloride, %	0.2	0.2
Soybean oil, %	5	11
Crude protein, %	17.7	53.4
Crude fat, %	5.1	11.4
Crude fiber, %	15.8	20.3
Crude ash, %	5.4	5.9
Starch, %	26.9	0.1
Sugar, %	9.9	—
NfE, %	51.7	1.9
Physiological fuel value, MJ/kg	13.6	13.6
Protein, kcal%	22	66
Fat, kcal%	14	32
Carbohydrates, kcal%	64	2

of *UCP2* or *OCNT2* in mice resulted in experimental colitis.[3,40,41] Conversely, conplastic mice with high mucosal OXPHOS and ATP levels have been already demonstrated by our group to be protected from experimental colitis.[42]

Apart from its role as a regulator of mitochondrial function, p32 has been described to interact with various proteins localized on the cell surface, the nucleus, the cytoplasm, or the extracellular space.[43] Binding of p32 to the globular heads of C1q reportedly inhibits classical pathway complement activation.[20] Furthermore, interaction of p32 with serum proteins involved in blood clotting and fibrin polymerization as well as binding to various bacterial or viral antigens[44] might play a role in the prevention of intestinal inflammation. Whether low levels of p32 observed in UC might lead to impairment in any of the mentioned pathways will be a topic of further investigations.

Here, we describe high level of KLF4-expressing terminally differentiated goblet cells as a healthy state and as necessary for mucus barrier integrity. In ATP8 mutant mice, carrying a mutation in complex V of the respiratory chain,

we observed low colonic expression of p32 accompanied by reduced klf4 mRNA expression, a diminished number of goblet cells and a thinned mucus layer. The transcription factor KLF4 specifically controls goblet cell fate, since in mice with intestinal deletion of *Klf4* both colonocytes and enteroendocrine cells appear to undergo normal maturation. Additionally, cell proliferation and cell death rates appear unchanged in *Klf4*-deficient mice, while goblet cell numbers are reduced by 90%.[16] In general, goblet cells are recognized to be a major line of defense in the intestinal mucosa. The 2-layered colonic mucus system separates bacteria from the host epithelium and the continuous self-renewal pushes bacteria out into the lumen, while animals with a penetrable mucus layer develop spontaneous colitis.[36] Notably, high KLF4 levels suppress development and progression of intestinal neoplasia and colitis-associated colorectal cancer upon azoxymethane or dextran sulfate sodium treatment in mice.[45]

Proliferation, rather than differentiation, of intestinal epithelial cells is highly important for tissue repair during

Figure 8. (*See previous page*). **GFHP diet increased mucosal energy supply, induced colonic p32 protein expression, and promoted goblet cell differentiation.** (*A*) Hypothesized metabolic switch upon GFHP dietary intervention in mice. Weekly (*B*) food consumption and (*C*) mice body weight was determined (n = 6 from 2 independent experiments). (*D*) Glucose and (*E*) L-lactate level were measured in serum samples from control and GFHP diet mice. Expression of transcripts was measured (*F*) via TaqMan probes for p32 exon 3–4 or (*I, K*) by SYBR qRT-PCR in colonic biopsies from control and GFHP diet mice. (*G, J*) Representative p32 (clone EPR8871) and KLF4-Alcian blue immunohistochemistry staining of paraformaldehyde-fixed colonic tissue samples as well as MUC2 fluorescent staining of Carnoy's fixed tissue are presented with corresponding quantifications.[51] Scale bar = 100 μM (10×), 50 μM (20×), 10 μM (63×). Arrow indicates inner mucus layer. (*H*) Western blot experiment of whole protein extracts from colonic samples from control and GFHP diet mice (p32 clone EPR8871). (*G, J*) (thickness of inner mucus layer) unpaired *t* test; (*I, J*) (KLF4 staining) unpaired *t* test with Welch's correction; results are shown as mean ± SD. *$P \le .05$.

Table 4. Information on Applied Primer Pairs and TaqMan Probes

Target gene	Forward primer (5′-3′)	Reverse primer (5′-3′)
Human		
ATOH1	CCAGCTGCGCAATGTTATCC	TGCTGTTTTCCTCCTGCACT
β-ACTIN	ACATCCGCAAAGACCTGTACG	TTGCTGATCCACATCTGCTGG
KLF4	CCATCTTTCTCCACGTTCG	ATCGGATAGGTGAAGCTGCA
Muc2	GACGGAGCTGAAGTTGGAAG	GGACACGGAGATGTTGGAGT
MUC5AC	CTGTGTCAAAGTGTGCCTGC	TTGATCACCACCACCGTCTG
p32	CTGCACACCGACGGAGACAA	CATATAAGGCCCAGTCCAAG
SPDEF1	GATTCACTACTGTGCCTCGAC	ATGTCTGGCTTCCGGATGAT
Mouse		
atoh1	GTGGGGTTGTAGTGGACGAG	GTTGCTCTCCGACATTGGG
β-actin	GATGCTCCCCGGGCTGTATT	GGGGTACTTCAGGGTCAGGA
cxcl1/kc	GCTGGGATTCACCTCAAGAA	TGGGGACACCTTTTAGCATC
ki67	CCTGCCCGACCCTACAAAAT	TTGCTCACACTCGATGCAGT
klf4	GATTAAGCAAGAGGCGGT	GGTAAGGTTTCTCGCCTGTG
lgr5	CGGCAACAGTGTGGACGACCT	GCGAGCACTGCACCGAGTGA
muc2	GCTGACGAGTGGTTGGTGAATG	GATGAGGTGGCAGACAGGAGAC
p32	CGCTCTGCACACGGAAGGAG	CGGCCTCATCTTCGTGTCCA
spdef1	GGAGAAGGCAGCATCAGGA	CCAGGGTCTGCTGTGATGT
Target genes	Exon-exon junction	Assay ID (Thermo Fisher Scientific)
Human β-ACTIN	Exon 1	Hs99999903_m1
Human p32	Exon 1	Hs05053979_g1
Human p32	Exon 1–2	Hs00241825_m1
Human p32	Exon 2-3	Hs00911223_g1
Human p32	Exon 3–4	Hs00911220_g1
Human p32	Exon 4–5	Hs00911221_g1
Human p32	Exon 5–6	Hs00911222_g1
Murine β-actin	Exon 2-3	Mm01205647_g1
Murine p32	Exon 3–4	Mm01245770_m1

active UC. Additionally, mitochondrial dysfunction in the colonic epithelium of patients with active UC has been reported to be accompanied by a reduction in fatty acid oxidation.[34] We have recently published that caspase-1 mediated cleavage of p32 results in a metabolic switch from mitochondrial oxidation to glycolysis, thereby shifting cell fate toward proliferation.[13] In line, mice deficient for caspase-1 display defects in mucosal tissue repair, being detrimental under dextran sulfate sodium–induced colitis, while derepression of the inflammasome complex results in enhanced repair and resistance to acute colitis.[46] Here, we demonstrate caspase-1 to be indeed activated in inflamed colonic tissue sections of UC patients, accompanied by a reduction of antibody binding against p32 exon 6 and a decrease of differentiated goblet cells. Taken together, loss of p32 in noninflamed colonic tissue appears highly problematic, owing to a decrease in differentiated goblet cells and thereby impaired mucus barrier function. Meanwhile, during colitis, p32 cleavage might be a physiologic mechanism necessary for induction of rapid cell proliferation for tissue repair.

We here propose nutritional intervention as a potential strategy to improve colonic p32 expression. A Westernized diet, rich in glucose, is a major environmental factor contributing to UC[47] and was found to continuously activate the NLRP3 inflammasome.[48,49] Having shown that caspase-1 mediated cleavage of p32 boosts cell proliferation,[13] we vice versa proposed an isocaloric GFHP diet to result in increased p32-mediated goblet cell differentiation. Indeed, mice receiving a GFHP diet exhibited induction of p32 protein expression in the colon, which was not due to elevated p32 mRNA level compared with control subjects. In line with human and in vitro data, GFHP mice depicted high mucosal energy level, an increased number of KLF4-positive terminally differentiated goblet cells, and a thickening of the colonic mucus layer compared with control subjects. Considering this, dietary intervention appears as a promising tool to modulate p32 expression, mitochondrial function, and goblet cell differentiation in the intestine.

In conclusion, we identified a new pathway linking low colonic expression of OXPHOS-regulating p32 to mitochondrial dysfunction, defective goblet cell differentiation, and impaired mucus barrier formation, frequently observed in UC. Furthermore, we present a diet low in glucose as an option to induce colonic expression of p32, opening new pathways in the preventive treatment and therapy of UC.

Materials and Methods

Study Cohort

Tissue biopsies from the terminal ileum and colon were obtained during endoscopy as part of regular patient management in the Medical Department 1, University Hospital Schleswig-Holstein, Campus Lübeck, Germany. Blood samples were collected at the University Hospital Schleswig-Holstein, Campus Lübeck; at the University Hospital Münster, North Rhine-Westphalia, Germany; and at the University Hospital Rostock, Mecklenburg Western Pomerania, Germany. Characteristics of histologically confirmed UC patients and non-IBD control subjects at time of endoscopy or sample collection are listed in Tables 1 and 2, respectively. The control group included patients who presented for a regular check-up or underwent endoscopy due to non–IBD-related reasons and presented without macroscopically and histological evidence of mucosal inflammation. Diagnosis of UC and classification of patients into remission and disease flare was based on clinical, endoscopic and histopathologic findings. Categorization into inflamed and noninflamed tissue was based on histopathologic presentation and activation of inflammasome component caspase-1. Groups were age and sex matched. Non-IBD control subjects or UC patients with reported colon cancer were excluded from the study. All patients gave informed consent for sample donation and protocols were approved by the ethics committees of the University of Lübeck (0-073; 03-043; AZ 13/084A; AZ 05-112), the University of Münster (AZ 2016-305-b-S), and the University of Rostock (A 2017-0137).

Animal Experiments

All animal experiments were approved by the ethics committee, Schleswig-Holstein, Germany (C57BL/6FVB: V 242-63560/2017 [5-1/18]; nutritional intervention: V 242-27664/2018 [64-5/17]). Mice were maintained at the University of Lübeck under specific pathogen-free conditions at a regular 12-hour light–dark cycle with free access to food (#1324; Altromin, Lage, Germany, if not indicated differently) and water. Procedures involving animals and their care were conducted in accordance with national and international laws and regulations.

C57BL/6J mice were obtained from the Jackson Laboratory (Bar Harbor, ME) and bred in the animal facility of the University of Lübeck. The conplastic strain C57BL/6J-mt$^{FVB/NJ}$, which carries a mutation in the mitochondrially encoded ATP8 mutant, was generated as described previously[30] and was maintained by repeatedly backcrossing female conplastic offspring with male C57BL/6J mice. Here, basal 2.5- to 4-months-old male ATP8 mutant mice and corresponding C57BL/6J control animals (B6 WT) were sampled in 3 independent rounds. Owing to differences in basal mRNA expression of targets of interest, expression data were normalized to average B6 WT target expression for each individual experiment. Colonoscopy was performed in sedated animals utilizing high-resolution mouse video endoscopy (Hopkins Optik 64019BA; Aida Vet; Karl Storz, Tuttlingen, Germany).

Glucose-free high-protein (GFHP) and isocaloric control diet were purchased from Ssniff (Soest, Germany). Compositions of corresponding diets are specified in Table 3. C57BL/6 mice were ordered at an age of 7–8 weeks from Charles River Laboratories (Wilmington, MA), were left to acclimatize on a standard chow diet until an age of 20 weeks and were than randomly distributed into GFHP diet– and isocaloric control diet–receiving groups. Mice were kept on the corresponding diet on an average of 70 days before sampling. Food consumption and body weight were measured once a week. Dietary intervention was performed in 2 independent experimental rounds.

Cell Culture

The human colorectal carcinoma cell lines HT29-MTX-E12 (Sigma-Aldrich, St Louis, MO) and DiFi[50] were kept in Dulbecco's modified Eagle medium (DMEM) medium supplemented with or without 1% nonessential amino acids, respectively. The human colorectal carcinoma cell line T84 was kindly provided by Markus Huber-Lang, University Hospital Ulm, Baden-Wuerttemberg, Germany, and grown in DMEM/F12 1:1 medium containing 1.5% HEPES. All cell culture media were supplemented with 10% (v/v) heat-inactivated fetal calf serum, 100-U/mL penicillin, and 100-mg/mL streptomycin. Cells were incubated at 37°C and 5% CO_2 in a humidified incubator. Cells were cultivated up to a maximum of 20 passages and confirmed to be negative for mycoplasma contamination every 3 months and when freshly thawed.

For terminal differentiation, HT29-MTX cells were either grown post confluent for 9 days as described previously[29] or stimulated with 1.25-mM butyrate (Merck Millipore, Burlington, MA) for 72 hours in the presence or absence of 1 μg/mL LPS-EB ultrapure (InvivoGen, San Diego, CA). DNP (Santa Cruz, Dallas, TX) or oligomycin (Agilent, Santa Clara, CA) were applied at indicated concentrations for 24 hours to inhibit mitochondrial respiration. Further, HT29-MTX cells were transiently transfected with 50-μM siRNA specific for human p32 (exon 3; s2138; Thermo Fisher Scientific) or control siRNA (Thermo Fisher Scientific) by reverse lipofection using lipofectamine 3000 reagent (Thermo Fisher Scientific) for 96 hours or were left untreated. After 24 hours, cells were stimulated with 1.25 mM butyrate for 72 hours or were left untreated.

RNA Extraction, Complementary DNA Synthesis, and Quantitative Reverse-Transcription Polymerase Chain Reaction

Isolation of total RNA from tissue biopsies or cell pellets was performed using the innuPREP RNA Mini Kit (Analytic Jena AG, Jena, Germany) according to manufacturer's guidelines. Additional DNA digestion was performed 2 times after binding of RNA to RNA column with 4 units DNase (Sigma-Aldrich) in according reaction buffer for 20 minutes at RT. For complementary DNA synthesis, 1 μg of

Table 5. Details of Applied Primary and Secondary Antibodies

Primary antibody	Species	Company	Working concentration
Anti-AMPKα (#2532)	rabbit	Cell Signaling Technology, Danvers, Massachusetts	1 μg/mL (WB)
Anti-α-TUBULIN (#2125)	rabbit	Cell Signaling Technology, Danvers, Massachusetts	1 μg/mL (WB)
Anti-β-ACTIN (#4967)	rabbit	Cell Signaling Technology, Danvers, Massachusetts	1 μg/mL (WB)
Anti-CASPASE-1 (#2225)	rabbit	Cell Signaling Technology, Danvers, Massachusetts	1:100 (IHC); 1:1000 (WB)[a]
Anti-mouse IgA α-chain (PAB9360)	rabbit	Abnova, Taipei, Taiwan	0.5 μg/mL (ELISA)
Anti-mouse Ig light chain κ (407201)	rat	BioLegend, San Diego, CA	1 μg/mL (ELISA)
Anti-mouse Ig light chain λ (407302)	rat	BioLegend, San Diego, CA	1 μg/mL (ELISA)
Anti-human KLF4 (AF3640)	goat	R&D Systems, Minneapolis, Minnesota	4 μg/mL (IHC); 1 μg/mL (WB)
Anti-murin KLF4 (AF3158)	goat	R&D Systems, Minneapolis, Minnesota	3.3 μg/mL (IHC)
Anti-MUC2 (clone H-300)	rabbit	Santa Cruz Biotechnologies, Dallas, Texas	2 μg/mL (IF)
Anti-Muc5AC (clone 45M1)	mouse	Bioss, Woburn, Massachusetts	2 μg/mL (IHC); 1 μg/mL (ELISA)
Anti-pAMPKα (Thr 172, #2535)	rabbit	Cell Signaling Technology, Danvers, Massachusetts	1 μg/mL (WB)
Anti-p32 (clone EPR8871)	rabbit	Abcam, Cambridge, United Kingdom	2 μg/mL (IHC); 0.4 μg/mL (WB)
Anti-p32 (clone 60.11)	mouse	Abcam, Cambridge, United Kingdom	1 μg/mL (WB)
Anti-p32 exon 6	rabbit	kindly provided by Berhane Ghebrehiwet	5 μg/mL (IHC)
Anti-TOMM22 (#WH0056993M1)	rabbit	Sigma-Aldrich, St Louis, Missouri	2.5 μg/mL (IHC)

Secondary antibodies/labeled polymers	Company	Working concentration
Alexa Fluor 594 nm goat anti rabbit	Thermo Fisher Scientific, Waltham, Massachusetts	8 μg/mL (IF)
Anti-mouse IgG HRP	Cell Signaling Technology, Danvers, Massachusetts	1:1000 (ELISA); 1:4000 (WB)[a]
Anti-rabbit IgG HRP	Cell Signaling Technology, Danvers, Massachusetts	1:2000 (ELISA); 1:4000 (WB)[a]
Anti-goat IgG HRP	Agilent, Santa Clara, California	1 μg/mL (IHC); 0.5 μg/mL (WB)
EnVision anti-rabbit HRP system	Agilent, Santa Clara, California	Not applicable
EnVision anti-mouse HRP system	Agilent, Santa Clara, California	Not applicable

ELISA, enzyme-linked immunosorbent assay; IHC, immunohistochemistry; WB, Western blot.
[a]If stock concentration was not provided by the manufacturer, dilution from stock solution was listed.

isolated RNA was transcribed with 100 pmol Oligo(dt)18 (Metabion, Steinkirchen, Germany), 20 U RiboLock RNase inhibitor (Thermo Fisher Scientific), dNTP Mix (0.2 mM for each dNTP), and 200 U RevertAid H Minus reverse transcriptase (Thermo Fisher Scientific) in corresponding reaction buffer at 42°C for 60 minutes. Target amplification was performed by quantitative reverse-transcription polymerase chain reaction on the StepOne real-time system (Thermo Fisher Scientific) applying Perfecta SYBR Green Supermix (Thermo Fisher Scientific) and 0.5-μM forward and reverse primer. Following cycling conditions were applied: initial denaturation at 95°C for 5 minutes; 40 cycles of denaturation at 95°C for 45 seconds, annealing at appropriate temperature (55°C) for 30 seconds and elongation for at 72°C for 30 seconds. Melting curve profiles were produced and data were analyzed following the 2^{-dCt} algorithm by normalized to β-actin. Primer sequences are listed in Table 4.

p32 exon expression was additionally analyzed by TaqMan probes (Thermo Fisher Scientific) (Table 4) according to manufacturer's instructions using the StepOnePlus Real-Time polymerase chain reaction system. The following cycling conditions were applied: preincubation at 50°C for 2 minutes and 95°C for 10 minutes, 40 cycles of denaturation at 95°C for 15 seconds, and annealing and elongation at 60°C for 1 minute. Ct-Values of targets were acquired via the StepOne system software and normalized to β-actin that served as an internal housekeeping transcript via the 2^{-dCT} algorithm.

Sodium Dodecyl Sulfate Polyacrylamide Gel Electrophoresis and Immunoblotting

Sodium dodecyl sulfate (SDS) polyacrylamide gel electrophoresis and immunoblotting was performed according to standard protocols. In short, whole-protein extracts from homogenized tissue samples or cells were prepared by cell lysis in denaturing lysis buffer containing 1% SDS, 10-mM Tris (pH 7.4), phosphatase II, phosphatase III, and protease inhibitor (Sigma-Aldrich). Protein extracts were separated by denaturing SDS polyacrylamide gel electrophoresis (Bio-Rad Laboratories, Hercules, CA) under reducing conditions and transferred onto polyvinylidene difluoride

membranes. After blocking, membranes were probed with specific primary antibodies followed by respective horseradish peroxidase (HRP)–conjugated secondary antibodies. To determine similar transfer and equal loading, membranes were stripped and reprobed with an appropriate housekeeper. Proteins of interest were visualized on a ChemiDoc XRS+ Imaging System (Bio-Rad Laboratories). Applied antibodies are listed in Table 5.

Histology and Microscopy Analyses

Immunohistochemical staining in paraformaldehyde-fixed and paraffin-embedded tissue biopsies was performed according to standard protocols. After deparaffinization, rehydration, endogenous peroxidase blockage, and antigen retrieval, tissue slides were probed with specific primary antibodies or isotype control antibodies, followed by respective HRP-conjugated secondary antibodies or HRP-labeled polymers (both listed in Table 5). Tissue slides were incubated with DAB-substrate (Dako, Jena, Germany) and counterstained with Mayer's hemalum solution or Alcian blue. Images were obtained and analyzed on an Axio Scope.A1 microscope (Zeiss, Oberkochen, Germany) utilizing the ZEN imaging software (Zeiss). If appropriate, stained areas were quantified via the color deconvolution plugin for the software ImageJ version 1.53e (National Institutes of Health, Bethesda, MD).[51]

For Muc2 immunofluorescent staining and quantification of mucus layer thickness, colonic biopsies were fixed in Carnoy's solution before paraffin-embedding. Slides were probed with specific antibodies for murine Muc2 or according isotype control, followed by incubation with respective fluorochrome-labeled IgG secondary antibody and counterstaining using DAPI (Sigma-Aldrich). Applied antibodies are listed in Table 5. Mucus layer thickness was measured at least at 4 different representative positions per slide per animal using the AxioCam software (Zeiss).

Enzyme-Linked Immunosorbent Assay

For detection of extracellular Muc5AC by enzyme-linked immunosorbent assay (ELISA), pure supernatant from cells was coated at 4°C overnight. Intracellular protein was detected in native protein isolates, coated with 50% coating buffer, containing 0.3% (w/v) $Na_2CO_3 \times 10\ H_2O$ and 0.6% (w/v) $NaHCO_3$, pH 9.6. After blocking, Muc5AC was detected using a Muc5AC-specific primary antibody in combination with a respective HRP-conjugated secondary antibody listed in Table 5. Optical density was measured at 450 nm against a reference wavelength of 540 nm on a SpectraMax iD3 microplate reader (Molecular Devices, San Jose, CA).

In order to quantify IgA in mouse fecal pellets, a sandwich ELISA was performed according to standard procedures. Applied antibodies are listed in Table 5. Fecal protein was extracted by homogenization in $10\times$ volume extraction buffer (20-mM Na_3PO_4, 650-mL NaCl, 1-mM EDTA, 1-mM PMSF, pH 7.4) per gram of feces. Coating of capture antibody against anti-mouse Ig light chain κ and λ was performed at 4°C overnight. Fecal protein extracts and

IgA RSG ELISA standard (Affymetrix, Santa Clara, CA) were diluted in 0.5% (w/v) bovine serum albumin and 0.05% (v/v) Tween 20 in PBS and applied for 2 hours at room temperature. After applying an anti-mouse IgA α-chain specific detection antibody followed by a respective HRP-conjugated secondary antibody, optical density was measured as described previously.

Seahorse Assay

For determination of OCR and ECAR via Seahorse assay, 5×10^3 HT29-MTX cells were seeded in a Seahorse XF24 cell culture plate in DMEM medium containing 5-mM glucose, 1% nonessential amino acids, 10% (v/v) heat-inactivated fetal calf serum, 100-U/mL penicillin, and 100-mg/mL streptomycin. Cells were stimulated with 1.25-mM butyrate for 72 hours or were left untreated. OCR and ECAR was determined in standard Seahorse medium on day 3 after seeding before and after injection of 2-μM oligomycin on a XF24 analyzer (Agilent) according to manufacturer's instructions.

Lactate Assay

L-lactate levels were measured in serum or plasma samples (1:5 diluted in PBS) and in cell culture supernatants (1:10 diluted in PBS) according to manufacturer's instructions (Megazyme, Wicklow, Ireland). Lactate level in cell culture supernatant were normalized to cell count.

Quantification of Mucosa Attached Bacteria

Extraction and quantification of mucosa-attached bacteria from mouse colonic tissue was performed as previously described.[52] In short, mucus was removed by incubation of biopsies in 500-μL PBS containing 0.016% DTT at 800 g for 1 minute. After wash, hypotonic lysis of eukaryotic cells was achieved by vortexing tissue in 500 μL ddH_2O at 800 g for 30 minutes. Bacteria and tissue debris were pelletized by centrifugation at 12,000 g for 3 minutes, taken up in 16% glycerol, and stored at –80°C. To quantify bacteria via flow cytometry, mucosa-attached bacteria were thawed on ice, washed with 1% (w/v) bovine serum albumin and 0.1% NaN_3 in PBS and incubated with 10-μM Syto BC green fluorescent nucleic acid stain (Thermo Fisher Scientific) for 20 minutes on ice. Flow cytometry was performed on an Attune NxT cytometer (Thermo Fisher Scientific) with a forward scatter threshold set to 10,000 to exclude cell debris from measurement.

Author Approval

All authors had access to the study data, reviewed and approved the final manuscript.

Statistics

Statistical analysis was performed using Prism version 6 (GraphPad, San Diego, CA). Outliers were identified by

Grubbs' test (significant level $\alpha = 0.05$). The F test was used to compare variances and D'Agostino–Pearson test was applied to test for normal distribution. Statistical differences between 2 groups were analyzed by unpaired t-test or paired t-test (normally distributed data), unpaired t test with Welch's correction (significant different variances) or Mann-Whitney U test (not-normally distributed data). For comparison of more than 2 groups, 1-way analysis of variance with Bonferroni posttest was applied. Uncorrected Fisher's least significant difference test was employed for datasets with 2 variables. Correlation analysis was performed by obtaining the Spearman's rank correlation coefficient. P values were calculated and null hypotheses were rejected when $P \leq .05$. Data are shown as mean ± 95% confidence interval, as mean ± SD for small datasets, or as median with interquartile range for datasets with large variances.

References

1. Ungaro R, Mehandru S, Allen PB, Peyrin-Biroulet L, Colombel JF. Ulcerative colitis. Lancet 2017; 389:1756–1770.
2. Stringari C, Edwards RA, Pate KT, Waterman ML, Donovan PJ, Gratton E. Metabolic trajectory of cellular differentiation in small intestine by Phasor fluorescence lifetime microscopy of NADH. Sci Rep 2012; 2:568.
3. Roediger WE. The colonic epithelium in ulcerative colitis: an energy-deficiency disease? Lancet 1980;2:712–715.
4. Sifroni KG, Damiani CR, Stoffel C, Cardoso MR, Ferreira GK, Jeremias IC, Rezin GT, Scaini G, Schuck PF, Dal-Pizzol F, Streck EL. Mitochondrial respiratory chain in the colonic mucosal of patients with ulcerative colitis. Mol Cell Biochem 2010;342:111–115.
5. Santhanam S, Rajamanickam S, Motamarry A, Ramakrishna BS, Amirtharaj JG, Ramachandran A, Pulimood A, Venkatraman A. Mitochondrial electron transport chain complex dysfunction in the colonic mucosa in ulcerative colitis. Inflamm Bowel Dis 2012; 18:2158–2168.
6. Pullan RD, Thomas GA, Rhodes M, Newcombe RG, Williams GT, Allen A, Rhodes J. Thickness of adherent mucus gel on colonic mucosa in humans and its relevance to colitis. Gut 1994;35:353–359.
7. Johansson ME. Mucus layers in inflammatory bowel disease. Inflamm Bowel Dis 2014;20:2124–2131.
8. Gersemann M, Becker S, Kubler I, Koslowski M, Wang G, Herrlinger KR, Griger J, Fritz P, Fellermann K, Schwab M, Wehkamp J, Stange EF. Differences in goblet cell differentiation between Crohn's disease and ulcerative colitis. Differentiation 2009;77:84–94.
9. McCormick DA, Horton LW, Mee AS. Mucin depletion in inflammatory bowel disease. J Clin Pathol 1990; 43:143–146.
10. Ito K, Suda T. Metabolic requirements for the maintenance of self-renewing stem cells. Nat Rev Mol Cell Biol 2014;15:243–256.
11. Kaiko GE, Ryu SH, Koues OI, Collins PL, Solnica-Krezel L, Pearce EJ, Pearce EL, Oltz EM, Stappenbeck TS. The colonic crypt protects stem cells from microbiota-derived metabolites. Cell 2016;167:1137.
12. Xu X, Duan S, Yi F, Ocampo A, Liu GH, Izpisua Belmonte JC. Mitochondrial regulation in pluripotent stem cells. Cell Metab 2013;18:325–332.
13. Sünderhauf A, Raschdorf A, Hicken H, Schlichting H. GC1qR cleavage by caspase-1 drives aerobic glycolysis in tumor cells. Front Oncol 2020;10:575854.
14. Yang Q, Bermingham NA, Finegold MJ, Zoghbi HY. Requirement of Math1 for secretory cell lineage commitment in the mouse intestine. Science 2001; 294:2155–2158.
15. Noah TK, Kazanjian A, Whitsett J, Shroyer NF. SAM pointed domain ETS factor (SPDEF) regulates terminal differentiation and maturation of intestinal goblet cells. Exp Cell Res 2010;316:452–465.
16. Katz JP, Perreault N, Goldstein BG, Lee CS, Labosky PA, Yang VW, Kaestner KH. The zinc-finger transcription factor Klf4 is required for terminal differentiation of goblet cells in the colon. Development 2002;129:2619–2628.
17. Gunther C, Neumann H, Neurath MF, Becker C. Apoptosis, necrosis and necroptosis: cell death regulation in the intestinal epithelium. Gut 2013;62:1062–1071.
18. Krainer AR, Mayeda A, Kozak D, Binns G. Functional expression of cloned human splicing factor SF2: homology to RNA-binding proteins, U1 70K, and Drosophila splicing regulators. Cell 1991;66:383–394.
19. Honore B, Madsen P, Rasmussen HH, Vandekerckhove J, Celis JE, Leffers H. Cloning and expression of a cDNA covering the complete coding region of the p32 subunit of human pre-mRNA splicing factor SF2. Gene 1993;134:283–287.
20. Ghebrehiwet B, Lim BL, Peerschke EI, Willis AC, Reid KB. Isolation, cDNA cloning, and overexpression of a 33-kD cell surface glycoprotein that binds to the globular "heads" of C1q. J Exp Med 1994; 179:1809–1821.
21. D'Souza M, Datta K. Evidence for naturally occurring hyaluronic acid binding protein in rat liver. Biochem Int 1985;10:43–51.
22. Fogal V, Richardson AD, Karmali PP, Scheffler IE, Smith JW, Ruoslahti E. Mitochondrial p32 protein is a critical regulator of tumor metabolism via maintenance of oxidative phosphorylation. Mol Cell Biol 2010; 30:1303–1318.
23. Yagi M, Uchiumi T, Takazaki S, Okuno B, Nomura M, Yoshida S, Kanki T, Kang D. p32/gC1qR is indispensable for fetal development and mitochondrial translation: importance of its RNA-binding ability. Nucleic Acids Res 2012;40:9717–9737.
24. Hillman GA, Henry MF. The yeast protein Mam33 functions in the assembly of the mitochondrial ribosome. J Biol Chem 2019;294:9813–9829.
25. Lonsdale J, Thomas J, Salvatore M, Phillips R, Lo E, Shad S, Hasz R, Walters G, Garcia F, Young N, Foster B, Moser M, Karasik E, Gillard B, Ramsey K, Sullivan S, Bridge J, Magazine H, Syron J, Fleming J, Siminoff L, Traino H, Mosavel M, Barker L, Jewell S, Rohrer D, Maxim D, Filkins D, Harbach P, Cortadillo E, Berghuis B, Turner L, Hudson E, Feenstra K, Sobin L, Robb J,

Branton P, Korzeniewski G, Shive C, Tabor D, Qi L, Groch K, Nampally S, Buia S, Zimmerman A, Smith A, Burges R, Robinson K, Valentino K, Bradbury D, Cosentino M, Diaz-Mayoral N, Kennedy M, Engel T, Williams P, Erickson K, Ardlie K, Winckler W, Getz G, DeLuca D, MacArthur D, Kellis M, Thomson A, Young T, Gelfand E, Donovan M, Meng Y, Grant G, Mash D, Marcus Y, Basile M, Liu J, Zhu J, Tu Z, Cox NJ, Nicolae DL, Gamazon ER, Im HK, Konkashbaev A, Pritchard J, Stevens M, Flutre T, Wen X, Dermitzakis ET, Lappalainen T, Guigo R, Monlong J, Sammeth M, Koller D, Battle A, Mostafavi S, McCarthy M, Rivas M, Maller J, Rusyn I, Nobel A, Wright F, Shabalin A, Feolo M, Sharopova N, Sturcke A, Paschal J, Anderson JM, Wilder EL, Derr LK, Green ED, Struewing JP, Temple G, Volpi S, Boyer JT, Thomson EJ, Guyer MS, Ng C, Abdallah A, Colantuoni D, Insel TR, Koester SE, Little AR, Bender PK, Lehner T, Yao Y, Compton CC, Vaught JB, Sawyer S, Lockhart NC, Demchok J, Moore HF. The Genotype-Tissue Expression (GTEx) project. Nat Genet 2013;45:580–585.

26. Sun N, Youle RJ, Finkel T. The mitochondrial basis of aging. Mol Cell 2016;61:654–666.

27. Schroll S, Sarlette A, Ahrens K, Manns MP, Goke M. Effects of azathioprine and its metabolites on repair mechanisms of the intestinal epithelium in vitro. Regul Pept 2005;131:1–11.

28. Lei-Leston AC, Murphy AG, Maloy KJ. Epithelial cell inflammasomes in intestinal immunity and inflammation. Front Immunol 2017;8:1168.

29. Navabi N, McGuckin MA, Linden SK. Gastrointestinal cell lines form polarized epithelia with an adherent mucus layer when cultured in semi-wet interfaces with mechanical stimulation. PLoS One 2013;8:e68761.

30. Yu X, Gimsa U, Wester-Rosenlof L, Kanitz E, Otten W, Kunz M, Ibrahim SM. Dissecting the effects of mtDNA variations on complex traits using mouse conplastic strains. Genome Res 2009;19:159–165.

31. Hirose M, Kunstner A, Schilf P, Sunderhauf A, Rupp J, Johren O, Schwaninger M, Sina C, Baines JF, Ibrahim SM. Mitochondrial gene polymorphism is associated with gut microbial communities in mice. Sci Rep 2017;7:15293.

32. Schroder T, Kucharczyk D, Bar F, Pagel R, Derer S, Jendrek ST, Sunderhauf A, Brethack AK, Hirose M, Moller S, Kunstner A, Bischof J, Weyers I, Heeren J, Koczan D, Schmid SM, Divanovic S, Giles DA, Adamski J, Fellermann K, Lehnert H, Kohl J, Ibrahim S, Sina C. Mitochondrial gene polymorphisms alter hepatic cellular energy metabolism and aggravate diet-induced nonalcoholic steatohepatitis. Mol Metab 2016;5:283–295.

33. Palm W, Thompson CB. Nutrient acquisition strategies of mammalian cells. Nature 2017;546:234–242.

34. Smith SA, Ogawa SA, Chau L, Whelan KA, Hamilton KE, Chen J, Tan L, Chen EZ, Keilbaugh S, Fogt F, Bewtra M, Braun J, Xavier RJ, Clish CB, Slaff B, Weljie AM, Bushman FD, Lewis JD, Li H, Master SR, Bennett MJ, Nakagawa H, Wu GD. Mitochondrial dysfunction in inflammatory bowel disease alters intestinal epithelial metabolism of hepatic acylcarnitines. J Clin Invest 2021; 131:e133371.

35. Khaloian S, Rath E, Hammoudi N, Gleisinger E, Blutke A, Giesbertz P, Berger E, Metwaly A, Waldschmitt N, Allez M, Haller D. Mitochondrial impairment drives intestinal stem cell transition into dysfunctional Paneth cells predicting Crohn's disease recurrence. Gut 2020;69:1939–1951.

36. Johansson ME, Gustafsson JK, Holmen-Larsson J, Jabbar KS, Xia L, Xu H, Ghishan FK, Carvalho FA, Gewirtz AT, Sjovall H, Hansson GC. Bacteria penetrate the normally impenetrable inner colon mucus layer in both murine colitis models and patients with ulcerative colitis. Gut 2014;63:281–291.

37. Ludikhuize MC, Meerlo M, Gallego MP, Xanthakis D, Burgaya Julia M, Nguyen NTB, Brombacher EC, Liv N, Maurice MM, Paik JH, Burgering BMT, Rodriguez Colman MJ. Mitochondria define intestinal stem cell differentiation downstream of a FOXO/notch axis. Cell Metab 2020;32:889–900.e7.

38. Yu X, Wieczorek S, Franke A, Yin H, Pierer M, Sina C, Karlsen TH, Boberg KM, Bergquist A, Kunz M, Witte T, Gross WL, Epplen JT, Alarcon-Riquelme ME, Schreiber S, Ibrahim SM. Association of UCP2 –866 G/A polymorphism with chronic inflammatory diseases. Genes Immun 2009;10:601–605.

39. Waller S, Tremelling M, Bredin F, Godfrey L, Howson J, Parkes M. Evidence for association of OCTN genes and IBD5 with ulcerative colitis. Gut 2006;55:809–814.

40. Zhang H, Kuai XY, Yu P, Lin L, Shi R. Protective role of uncoupling protein-2 against dextran sodium sulfate-induced colitis. J Gastroenterol Hepatol 2012;27:603–608.

41. Shekhawat PS, Srinivas SR, Matern D, Bennett MJ, Boriack R, George V, Xu H, Prasad PD, Roon P, Ganapathy V. Spontaneous development of intestinal and colonic atrophy and inflammation in the carnitine-deficient jvs (OCTN2(-/-)) mice. Mol Genet Metab 2007;92:315–324.

42. Bar F, Bochmann W, Widok A, von Medem K, Pagel R, Hirose M, Yu X, Kalies K, Konig P, Bohm R, Herdegen T, Reinicke AT, Buning J, Lehnert H, Fellermann K, Ibrahim S, Sina C. Mitochondrial gene polymorphisms that protect mice from colitis. Gastroenterology 2013;145:1055–1063.e3.

43. Saha P, Datta K. Multi-functional, multicompartmental hyaluronan-binding protein 1 (HABP1/p32/gC1qR): implication in cancer progression and metastasis. Oncotarget 2018;9:10784–10807.

44. Peerschke EI, Ghebrehiwet B. The contribution of gC1qR/p33 in infection and inflammation. Immunobiology 2007;212:333–342.

45. Yang VW, Liu Y, Kim J, Shroyer KR, Bialkowska AB. Increased genetic instability and accelerated progression of colitis-associated colorectal cancer through intestinal epithelium-specific deletion of Klf4. Mol Cancer Res 2019;17:165–176.

46. Dupaul-Chicoine J, Yeretssian G, Doiron K, Bergstrom KS, McIntire CR, LeBlanc PM, Meunier C, Turbide C, Gros P, Beauchemin N, Vallance BA, Saleh M. Control of intestinal homeostasis, colitis, and colitis-associated colorectal cancer by the inflammatory caspases. Immunity 2010;32:367–378.

47. Rizzello F, Spisni E, Giovanardi E, Imbesi V, Salice M, Alvisi P, Valerii MC, Gionchetti P. Implications of the Westernized diet in the onset and progression of IBD. Nutrients 2019;11:1033.

48. Ahechu P, Zozaya G, Marti P, Hernandez-Lizoain JL, Baixauli J, Unamuno X, Fruhbeck G, Catalan V. NLRP3 inflammasome: a possible link between obesity-associated low-grade chronic inflammation and colorectal cancer development. Front Immunol 2018; 9:2918.

49. Christ A, Gunther P, Lauterbach MAR, Duewell P, Biswas D, Pelka K, Scholz CJ, Oosting M, Haendler K, Bassler K, Klee K, Schulte-Schrepping J, Ulas T, Moorlag S, Kumar V, Park MH, Joosten LAB, Groh LA, Riksen NP, Espevik T, Schlitzer A, Li Y, Fitzgerald ML, Netea MG, Schultze JL, Latz E. Western diet triggers NLRP3-dependent innate immune reprogramming. Cell 2018;172:162–175.e14.

50. Olive M, Untawale S, Coffey RJ, Siciliano MJ, Wildrick DM, Fritsche H, Pathak S, Cherry LM, Blick M, Lointier P, Roubein LD, Levin B, Boman BM. Characterization of the DiFi rectal carcinoma cell line derived from a familial adenomatous polyposis patient. vitro Cell Dev Biol 1993;29A:239–248.

51. Ruifrok AC, Johnston DA. Quantification of histochemical staining by color deconvolution. Anal Quant Cytol Histol 2001;23:291–299.

52. Sunderhauf A, Skibbe K, Preisker S, Ebbert K, Verschoor A, Karsten CM, Kemper C, Huber-Lang M, Basic M, Bleich A, Buning J, Fellermann K, Sina C, Derer S. Regulation of epithelial cell expressed C3 in the intestine - relevance for the pathophysiology of inflammatory bowel disease? Mol Immunol 2017;90:227–238.

53. Reef S, Shifman O, Oren M, Kimchi A. The autophagic inducer smARF interacts with and is stabilized by the mitochondrial p32 protein. Oncogene 2007;26:6677–6683.

Correspondence
Address correspondence to: Stefanie Derer, PhD, Division of Nutritional Medicine, University Hospital Schleswig-Holstein, Campus Lübeck, Ratzeburger Allee 160, 23538 Lübeck, Germany. e-mail: stefanie.derer@uksh.de; fax: +49(0)451/3101 8404. OR Christian Sina, MD, Division of Nutritional Medicine, University Hospital Schleswig-Holstein, Campus Lübeck, Ratzeburger Allee 160, 23538 Lübeck, Germany. e-mail: christian.sina@uksh.de; fax: +49(0)451/3101 8404.